CONFIDENTIAL

Copy
RM L9G06a

NACA RM L9G06a

NACA

RESEARCH MEMORANDUM

INVESTIGATION OF THE NACA 4-(5)(08)-03 TWO-BLADE PROPELLER AT FORWARD MACH NUMBERS TO 0.925

By James B. Delano and Melvin M. Carmel

Langley Aeronautical Laboratory
Langley Air Force Base, Va.

NATIONAL ADVISORY COMMITTEE FOR AERONAUTICS

WASHINGTON

September 15, 1949

CONFIDENTIAL

NATIONAL ADVISORY COMMITTEE FOR AERONAUTICS

RESEARCH MEMORANDUM

INVESTIGATION OF THE NACA 4-(5)(08)-03 TWO-BLADE PROPELLER AT FORWARD MACH NUMBERS TO 0.925

By James B. Delano and Melvin M. Carmel

SUMMARY

Investigations of the NACA 4-(5)(08)-03 two-blade propeller have been made in the Langley 8-foot high-speed tunnel for blade angles from 20° to 70° for forward Mach numbers up to 0.925.

The results show that the adverse effects of compressibility may be delayed to a forward Mach number of 0.71 for a blade angle of 65° for which the maximum efficiency was found to be 88 percent. At supercritical forward Mach numbers the rate of maximum efficiency loss increases with an increase in blade angle, and maximum efficiencies greater than 56 percent may be obtained at a forward Mach number of 0.925 for blade angles less than 55°. When adverse compressibility effects can no longer be delayed, the advance ratio must be decreased to obtain the highest maximum efficiencies. For very high supercritical Mach numbers, operation at reduced advance ratios provides an increase in efficiency through increased values of lift-drag ratios for the blade sections, but the principal gain in efficiency is due to a more favorable geometry of the force vectors. These results are in good agreement with theory and also indicate that supersonic types of propellers appear to be the most promising in the high subsonic speed range with regard to obtaining the highest possible efficiency. Consideration of the propeller when operating in the supersonic range indicates very favorable power-absorbing characteristics so that a relatively much smaller supersonic propeller may be used to absorb the same power at a Mach number of 0.9 than would be necessary at a Mach number of 0.75.

INTRODUCTION

High-speed investigations of propellers have been made previously at forward Mach numbers up to 0.725. Many airplanes are now being designed, however, to fly at much greater Mach numbers. Consequently,

an investigation of the NACA 4-(5)(08)-03 two-blade propeller reported in reference 1 was begun to obtain propeller performance at transonic speeds. That investigation was not complete because of power limitations and mechanical difficulties encountered with the propeller dynamometer. Since that investigation, the dynamometer was redesigned and the investigation has been completed.

Presented herein are the force-test results of the NACA 4-(5)(08)-03 two-blade propeller covering a complete range of blade angle from 20° to 70° for a forward Mach number range from 0.175 to 0.925. These results constitute the first part of a general propeller program intended to study the effects of blade-thickness ratio, section camber, blade sweep, and dual rotation on the performance of propellers operating at transonic speeds. Only a limited analysis of the force-test results is presented at this time to expedite publication of the basic propeller results. Inasmuch as the present investigation is much more extensive and the measurements are believed to be more accurate than those of reference 1, these data should supersede those presented in reference 1. Large-scale plots of the basic propeller characteristics (fig. 10) are available on request to the NACA.

SYMBOLS

A	area used in thrust-tare calculation, square feet
B	number of blades
b	blade width, feet
c_{l_d}	section design lift coefficient
C_P	power coefficient $\left(\frac{P}{\rho n^3 D^5}\right)$
C_T	thrust coefficient $\left(\frac{T}{\rho n^2 D^4}\right)$
D	propeller diameter, feet, or drag, pounds
b/D	blade-width ratio
D_{f_T}	skin friction of spinner (no propeller), pounds

D_{f_P}	skin friction of spinner (with propeller), pounds
h	maximum thickness of blade section, feet
h/b	blade–thickness ratio
J	advance ratio $\left(\frac{V_o}{nD}\right)$
L	lift, pounds
M	tunnel–datum (forward) Mach number (tunnel Mach number uncorrected for tunnel–wall constraint)
M_L	local Mach number
M_t	helical–tip Mach number $\left(M\sqrt{1 + \left(\frac{\pi}{J}\right)^2}\right)$
n	propeller rotational speed, revolutions per second
P	power, foot–pounds per second
Δp_T	change in static pressure without propeller, pounds per square foot
Δp_P	change in static pressure with propeller, pounds per square foot
q	dynamic pressure $\left(\frac{\rho V^2}{2}\right)$
R	propeller–tip radius, feet
r	blade–section radius, feet
T	thrust, pounds
T_c	thrust disk–loading coefficient $\left(\frac{T}{2qD^2}\right)$
T_T	indicated thrust (no propeller), pounds
T_P	indicated thrust (with propeller), pounds

V	tunnel-datum velocity (tunnel velocity uncorrected for tunnel-wall constraint), feet per second
V_o	equivalent free-air velocity (tunnel-datum velocity corrected for tunnel-wall constraint), feet per second
V_w	velocity in wake, feet per second
x	blade-section station (r/R)
α_i	induced angle of attack
β	section blade angle, degrees
$\beta_{0.75R}$	blade angle at 0.75 radius, degrees
γ	$\cot^{-1}$ (lift-drag ratio for two-dimensional flow)
η	efficiency $\left(\frac{J c_T}{c_P}\right)$
η_{max}	maximum efficiency
ρ	air density, slugs per cubic foot
ϕ_o	geometric helix angle $\left(\tan^{-1}\frac{J}{\pi x}\right)$

APPARATUS, CALIBRATIONS, AND METHODS

Test Equipment

This investigation was conducted in the Langley 8-foot high-speed tunnel. The nozzle of this tunnel provides both a subsonic and a supersonic test section. The propeller dynamometer was installed in the tunnel as shown in figure 1. The propeller was located in the subsonic test section of the nozzle.

Dynamometer.— The primary structure of the dynamometer consists of a long circular shell 13 inches in diameter and $1\frac{1}{4}$ inches thick. It is built in two similar units so that either single— or dual—rotation propellers can be tested. Each unit is supported by a large—chord strut at its center. The dynamometer has a nominal rating of 800 horsepower at 5400 revolutions per minute and can be overloaded for short periods of time. A continuous speed control for the four induction motors which drive the propeller is obtained by the use of a variable—frequency power supply. Each unit has two motors flexibly coupled. Sectional views of the dynamometer are shown in figure 2 and a detailed description of this dynamometer is presented in appendix A.

Calibrations

The calibration of the tunnel air stream consisted principally of longitudinal surveys of the static—pressure and radial surveys of the static and total pressures in the propeller test plane.

Longitudinal survey.— The longitudinal static—pressure surveys were made by the use of a tube 12 feet in length which was installed first 6 inches and then 18 inches below and parallel to the outer surface of the dynamometer barrel. Flush static—pressure orifices along the surface of this tube provided measurement of the static pressure from which the values of Mach number were obtained. The longitudinal Mach number distributions obtained 18 inches below the dynamometer surface are presented in figure 3. The pressure distributions at 6 and 18 inches from the dynamometer barrel were the same.

Radial survey.— The radial distribution of Mach number was measured with two survey rakes shown in figure 1. For these surveys the rakes were moved forward of the position shown in the figure to obtain measurements in the propeller plane. The Mach number distribution was uniform across the propeller plane and the maximum variation in Mach number was less than ± 0.0005, which is the order of accuracy of the measurement. The pressure measurements with the 12—foot tube checked the radial survey at both the 6— and 18—inch positions.

Horizontal survey.— A horizontal survey rake located 6.5 inches above the dynamometer barrel at the propeller plane was used to measure the velocity distribution in the wake of the front dynamometer support strut. The velocity distribution obtained is shown in figure 4. Calculations of the effects of this variation in velocity on the average stream velocity show it to be negligible.

Thrust and torque calibrations.— Typical results of the thrust and torque calibrations for the dynamometer are presented in figure 5. In the important range of propeller thrust and torque measured in this investigation the maximum error in indicated thrust and torque was less than 0.25 percent of the applied load. In the very small load range somewhat greater errors are involved. The method for measuring the propeller rotational speed is described in appendix A. The measured rotational speeds are accurate to within ±2 revolutions per minute for all rotational speeds.

Propeller and Tests

Propeller.— The NACA 4-(5)(08)-03 two-blade propeller used in this investigation is the same propeller as that used in the investigations reported in references 1 and 2. The blade was designed for a three-blade propeller to produce minimum induced energy losses (profile drag assumed equal to zero) at a blade angle of 45° at the 0.7-radius station and at an advance ratio of 2.1. The gaps between the spinner and blades were sealed for all operating conditions. Blade-form curves are shown in figure 6. A photograph of the blades investigated is shown in figure 7.

Tests.— Thrust, torque and rotational speed were measured throughout the complete operating range of the propeller. For each tunnel Mach number the propeller was run at constant blade angle and the rotational speed was varied. The range of blade angle covered for each test Mach number is given in the following table:

TABLE

Forward Mach number M	Blade angle at 0.75 radius, $\beta_{0.75R}$, deg										
0.175	20	25	30		40	45					
.23	20	25	30	35		45					
.35		25	30	35	40		50		60		
.43			30	35	40	45		55		65	70
.53					40	45	50			65	
.60					40	45	50	55		65	
.65						45	50	55	60		70
.70						45	50	55	60	65	70
.75						45	50	55	60	65	70
.80							50	55	60	65	70
.85								55	60	65	70
.90								55	60	65	70
.925								55	60	65	70

REDUCTION OF DATA

Propeller thrust.– Propeller thrust, as used in this report, is defined as the shaft tension produced by the spinner–to–tip portion of the blade. In order to obtain propeller thrust, it was necessary to determine thrust tares with the dynamometer operating without the propeller for all rotational speeds and forward Mach numbers at which the propeller would be operating. In addition, the changes in thrust force produced by the changes in pressures in the spinner gap in the presence of the operating propeller and in the dynamometer housing were measured and applied as corrections to the measured thrust. The corrections to the measured thrust due to spinner–skin–friction tares are presented in figure 8. A detailed description of the method used to obtain the actual propeller thrust is given in appendix B.

Propeller torque.– Torque–tare corrections were found to be small and dependent on spinner rotational speed. The indicated torque reading was corrected for the spinner tare (a maximum of 1.2 foot–pounds at 6000 rpm).

Tunnel–wall correction.– The force–test data have been corrected for the effect of tunnel–wall constraint on velocity at the propeller test plane. The method generally used for determining the effects of tunnel–wall constraint (reference 3) has consisted of measurement of

the air-stream velocity along radial lines from the propeller tip to the tunnel wall immediately ahead of and behind the propeller plane. The equivalent free-air velocity was then obtained by extrapolation of these measurements to an imaginary point beyond the tunnel wall where the two sets of fore and aft measurements led to the same value of velocity.

The uncertainty in the determination of the asymptotic value of velocity plus the difficulty in procuring survey rakes which would be structurally suitable at transonic speeds and which would be satisfactory as regards aerodynamic interference and choking effects led to the consideration of another method for the determination of the wall-interference effects. This method is based upon the measurement of the effect of propeller operation on the pressures along the tunnel wall. The equivalent free-air velocity is determined by taking one-half of the maximum difference between the tunnel-wall velocity with the propeller off and the tunnel-wall velocity with the propeller operating and applying this increment to the tunnel-datum velocity for the propeller-off condition. This approach to the problem has its basis in the propeller-momentum theory (reference 4) which shows that the induced velocity at the propeller plane has a value of one-half the induced velocity in the final wake.

The pressure measurements along the tunnel wall showed that the maximum change in tunnel-wall velocity, due to the propeller, occurred approximately 0.8 propeller diameter downstream of the propeller. Confirmation of the validity of the method used was indicated by the result that the measured velocity increments along the tunnel wall at the propeller plane were one-half of the maximum velocity increments downstream of the propeller. The results of these measurements are presented in figure 9 as the ratio of the free-air velocity to the tunnel-datum velocity as a function of the thrust disk-loading coefficient and the tunnel-datum Mach number. Further confirmation of the validity of this method of evaluating the tunnel-wall-interference correction is indicated by the agreement between the experimentally determined values and the theoretical values obtained from the method of reference 5. For the purpose of this paper, the agreement between the experimental and theoretical correction is presented in lieu of a formal proof of the method used.

Accuracy of results.- Analysis of the accuracy of the separate measurements previously described has indicated that errors in the results presented herein are probably less than 1 percent. Repeat runs have confirmed this estimate.

RESULTS AND DISCUSSION

The basic propeller characteristics are presented in figure 10. For each value of tunnel-datum Mach number, M, the propeller thrust and power coefficients and efficiency are plotted against advance ratio. The variation of tip Mach number with advance ratio is also included. As used in this report, the tunnel-datum Mach number, M, is not corrected for tunnel-wall constraint. However, the free-stream Mach number can be obtained by applying the tunnel-wall corrections, presented in figure 9, to the tunnel-datum Mach number. At the high Mach numbers the tunnel-wall correction is generally less than 1 percent but, in any rigorous analysis wherever small changes in Mach number produce large changes in propeller characteristics involving the basic data presented in figure 10, the tunnel-datum Mach number should be corrected to free-stream Mach number.

Effect of forward Mach number on maximum efficiency.- The variation of maximum efficiency with forward Mach number is presented in figure 11 for all of the blade angles investigated. The dashed lines, which provide an estimation of the data for the lower blade angles, represent merely the highest measured values of efficiency and do not represent the highest possible values of the efficiency.

The highest values of low-speed maximum efficiency were obtained throughout a wide range of blade angles from 30° to 60°. The maximum efficiency throughout this range was about 92 percent. At blade angles above 60°, and particularly at the blade-angle setting of 70°, large reductions in the value of the efficiency resulted (η = 84 percent). These relatively low efficiency values for the higher blade angles are undoubtedly due to the high rotational losses associated with the high blade-angle operation which are further aggravated by the fact that the design pitch distribution for these blades (design β = 45°) leads to operation of the shank sections at blade angles greater than 90°. As has been shown previously, the forward Mach number at which efficiency losses begin because of adverse effects of compressibility was found to increase with increase in blade angle. For this propeller, these adverse effects were delayed to a forward Mach number of 0.71 for which a blade angle of 65° was required. The maximum efficiency for this condition was 88 percent. Beyond this point the large low-speed losses previously discussed for the 70° case become even greater and thus limit any further delays in compressibility effects through the use of higher blade angles. These delays are accomplished simply through the reduction in rotational speed as the forward speed is increased to maintain sufficiently low tip speeds to avoid the effects of compressibility. Once the effects of compressibility occur, however, large reductions in the efficiency associated with reduced lift-drag ratios are encountered for all the blade angles tested. The rate of maximum

efficiency reduction increases as the blade angle is increased. At a forward Mach number of 0.9 the value of maximum efficiency is 57 percent at a blade angle of 55°.

Attention is called to the fact that in the range of forward Mach numbers above approximately 0.8 the maximum values of efficiency are obtained for the lowest values of blade angle which correspond to the lowest values of advance–diameter ratio, and thus in this speed range, decreases in the advance–diameter ratio rather than increases in advance–diameter ratio appear necessary for best efficiency. Further attention is called to the fact that these lower values of blade angle and the corresponding reductions in advance–diameter ratio are associated with marked increases in rotational speeds so that the propeller, at a blade angle of 55° and at a forward Mach number of 0.925, is operating almost as a fully supersonic propeller in which the resultant Mach numbers all along the blade are in excess of unity ($M_t \approx 1.5$). The results therefore indicate that supersonic types of propellers appear to be most promising in the high subsonic speed range with regard to obtaining the highest possible efficiency.

Effect of advance ratio and forward Mach number on maximum efficiency.– A further insight into the nature of this phenomenon is gained by considering as a primary variable the advance ratio. These same maximum efficiency results from figure 11 are presented as solid-line curves in figure 12. For purposes of comparison, calculated values of propeller efficiency are also shown for fixed values of the lift–drag ratio L/D in the form of dashed lines.

The efficiency of a section along the blade is a function of the geometric helix angle, induced angle of attack, and the two-dimensional lift–drag ratio, and is given by

$$\eta_x = \tan \phi_o \operatorname{cotan}(\phi_o + \alpha_i + \gamma) \tag{1}$$

If α_i and γ are combined, it is possible to define a new lift–drag ratio which includes induced drag and is therefore comparable to the definition of lift–drag ratio for a finite wing. In this paper the lift–drag ratio is therefore defined by

$$\alpha_i + \gamma = \operatorname{cotan}^{-1} \frac{L}{D} \tag{2}$$

Since the geometric helix angle is given by

$$\phi_o = \tan^{-1} \frac{J}{\pi x} \tag{3}$$

the section efficiency can be expressed as

$$\eta_x = \frac{1 - \left(\frac{J}{\pi x}\right)\left(\frac{1}{\frac{L}{D}}\right)}{1 + \frac{1}{\left(\frac{J}{\pi x}\right)\left(\frac{L}{D}\right)}} \tag{4}$$

The theoretical section efficiency given by equation (4) has been plotted in figure 12 for the 0.7-radius station and thus represents an approximate average propeller efficiency. Both the experimental results and the calculated results show that, when the levels of efficiency are high (corresponding to high values of lift-drag ratios), a wide range of advance ratio exists through which high levels of efficiency are maintained. As the Mach number is increased, however, there first occur the reductions in the efficiency in the lower range of advance-diameter ratios due to the onset of compressibility effects in the experimental results; thus, only a narrow region of high values of the advance ratio are left for which high values of efficiency are obtained. With further increases in Mach number, however, even this small range of high advance ratio is eliminated, and the average values of the blade L/D as indicated by comparison with the dashed lines undergo marked reductions.

At the low values of advance ratio the theory clearly indicates that the efficiency is no longer relatively insensitive to the value of J as was previously pointed out for the low-speed operating cases. Examination of the theory to explain the sensitivity of the efficiency to advance ratio when the values of lift-drag ratio are low has indicated that this gain is associated with the changes in the geometrical combination of the force vectors. The theoretical line for lift-drag ratios of 3 and 4 shows that very marked differences in efficiency occur over the range of advance ratios investigated by the experimental study. The reduction thus obtained from the theoretical calculation would indicate that for a fixed value of lift-drag ratio, advance ratios of the order of 2 are necessary to maintain best possible efficiencies. The experimental results tend to confirm this at forward Mach numbers in the range around 0.9. The comparison between the theoretical and the experimental results further indicates that about three-fourths of

the rise in efficiency with reduction of the advance–diameter ratio shown in the experimental results is accounted for solely by the reduction in J. The slightly greater slope for the experimental results, accounting for the remaining 25 percent of the improved efficiency, is chargeable to slight improvements in the average lift–drag ratio.

The results of the analytical study have therefore confirmed the experimental indication that operation at lower advance ratios at very high subsonic forward Mach numbers (supersonic operation) would be expected to give the best possible propeller performance.

Power coefficient for maximum efficiency.– Contours of constant power coefficient for maximum efficiency are shown as dashed lines in figure 13. The solid lines are the maximum efficiency results from figure 11. At the highest forward Mach numbers reached in this investigation, the power coefficient for highest efficiency decreased to about half the values occurring at forward Mach numbers of about 0.75. These very marked reductions in power coefficient are, however, associated with quite large reductions in the size of the propellers needed for maximum efficiency in the higher speed range. For example, although there is a marked reduction in the power coefficient for maximum efficiency, the actual power absorption of this two–blade propeller at an advance ratio of 2.8 and at a forward Mach number of 0.9 is six times as great as the corresponding power absorption of the propeller when operating at a forward Mach number of 0.75 and an advance ratio of approximately 5. Thus a very much smaller propeller is required for the supersonic type of propeller; and if this comparison is based upon consideration of propellers of different size to absorb the same power, it would result in the supersonic propeller operating at a Mach number of 0.9 which would have a diameter 40 percent of the diameter of the subsonic propeller designed to absorb the same power at a forward Mach number of 0.75. Thus, a very favorable power–absorption characteristic is indicated for the low advance–ratio supersonic type of propeller, which would lead to considerable reduction in propeller weight.

Comparison with results of previous investigation.– The envelope efficiencies for blade angles of 45° and 60° are presented in figure 14 and compared with results of the previous investigation reported in reference 1.

The keyed symbols in figure 14 are included to indicate the points of tangency of the envelope curve with the individual efficiency curves for a given forward Mach number. The dashed line in the curve for the 60° blade angle of reference 1 represents the highest measured efficiencies, but the limited range of power available in the previous tests was insufficient to reach the maximum–efficiency conditions; thus, in this

range, the differences in the two sets of data result primarily from the increased power available in the present tests. The remaining comparisons, that is, for the 45° blade angle and the lower-speed range for the 60° blade angle, generally present an average difference of the order of about 3 to 4 percent. This difference is believed to result primarily from the combined errors in the testing techniques of the two series of tests. In the former tests, the measurements were considerably less accurate than in the current tests and, as is noted in reference 1, determination of the efficiencies was not believed to be more accurate than about 2 percent with the possibility of errors due to spinner corrections of an additional 1 percent, thus about 3 percent of the difference can be considered chargeable to the errors of the previous tests. Because the present tests are considered to represent a much more accurate set of measurements and are much more extensive, it is recommended that the results presented in this paper be considered to supersede the results of reference 1.

CONCLUSIONS

Tests of an NACA 4-(5)-(08)-03 two-blade propeller in the Langley 8-foot high-speed tunnel for blade angles of 20° to 70° and through a forward Mach number range extending up to 0.925 indicate the following results:

1. The adverse effects of compressibility may be delayed to a maximum forward Mach number of 0.71 for a blade angle of 65° for which the maximum efficiency was found to be 88 percent.

2. For the forward Mach numbers at which low lift-drag ratios due to operation at supercritical speeds can no longer be avoided, the highest efficiencies are obtained at reduced values of advance ratio, approximately 2.0 for best efficiency.

3. At high supercritical forward Mach numbers, large gains in maximum efficiency are possible through operation at low advance ratios. Part of this efficiency gain results from increased blade-section lift-drag ratio, but the principal gain results from the more favorable geometry of the force vectors. For these conditions of operation, which are obtained through large increases in rotational speed, the propeller operates as a supersonic propeller.

4. Consideration of the propeller when operating at supersonic section speeds indicates very favorable power-absorbing characteristics so that a relatively much smaller supersonic propeller may be used to

obtain the same power-absorbing characteristics at a Mach number of 0.9 than would be necessary to absorb the same power at a forward Mach number of 0.75.

Langley Aeronautical Laboratory
National Advisory Committee for Aeronautics
Langley Air Force Base, Va.

APPENDIX A

DESCRIPTION OF PROPELLER DYNAMOMETER

Figure 1 shows the complete dynamometer installed in the test section of the tunnel. Figure 2 shows one of the two similar 400-horsepower units of the dynamometer. The two motors of each unit are "doubly" coupled; that is, a flexible coupling connects the drive shafts or rotors and a fixed coupling connects the two stators or motor casings so that each unit has essentially one motor of 400 horsepower. The fixed coupling is a long steel shell. On each end of this shell a cylindrical air bearing (shown in fig. 2(b), detail A) 10 inches long and $8\frac{1}{2}$ inches in diameter supports all the moving parts of one unit. The air bearing is essentially a thin jacket of moving air which provides the sustaining force for the dynamometer. The outer race of this bearing is fixed to the outer shell of the dynamometer and contains a compressed-air chamber and a system of radial orifices located longitudinally and circumferentially around the race. The inner race is a floating sleeve which is connected to the motor casings by an alinement ring. Between the two races is a gap of about 0.002 inch through which the compressed air (pumped from an external source) is allowed to expand. This air flows out both ends of the air bearing and is deflected by exhaust-air baffles to flow over the coupling shell and out through the large supporting struts and then into the tunnel (fig. 1). A labyrinth-type seal located at the end of the dynamometer unit near the propeller restricts the flow of air out of that end of the dynamometer. One part of this seal was fixed to the outside casing of the dynamometer and the other part was fixed to the floating unit of the dynamometer.

Axial and rotational movement of the floating parts of the dynamometer is automatically controlled by pneumatic compensators to provide essentially a null-movement system. These pneumatic compensators are integral parts of the hydraulic thrust- and torque-measuring units.

A cross section of the torque unit is shown in figure 2(c), detail B. Two semicircular shells and two flat air plates containing a compressed-air chamber are rigidly connected to the outer casing of the motors. The air escapes from the air chamber through small orifices in the plates. Between the air plates is a four-cell hydraulic cylinder block rigidly fixed to the outer barrel of the dynamometer. The liquid in each hydraulic capsule is retained by a rubber diaphragm against which a floating piston acts to change the pressure of the fluid when a torque force is transmitted to it. An air gap of 0.002 inch exists

between the outer surfaces of the pistons and the air plates on the semicircular shell. This film of air transmits the motor-torque reaction to the pistons of the hydraulic units. When the semicircular shells move rotationally, because of torque reaction, the pressures in the air gaps change, and thereby produce corresponding changes in the load on the pistons. Diametrically opposite pistons experience identical changes in pressure, and the hydraulic fluid acted upon by diametrically opposite pistons is forced into one hydraulic pressure line leading to one side of a similar hydraulic capsule on a Toledo Printweigh scale. The pressure line from the other two hydraulic capsules in the dynamometer is connected similarly to the other side of a hydraulic capsule on the beam balance.

The fluid in each of these hydraulic units is supplied from separate reservoirs which are kept about half full. The upper part of one reservoir contains air maintained at a constant pressure through a constant-pressure valve inserted in the air-supply line. The upper part of the other reservoir contains pressure-regulated air from a pilot valve. This pilot valve is connected directly to the air-supply line and to a compensator valve which automatically fixes the position of the floating part of the dynamometer and regulates the pressure in the reservoir for all applied torque loads. The pressure difference between the two hydraulic units is proportional to the torque and is measured directly on the beam balance.

Operation of the thrust unit (see fig. 2(c), detail C) is similar to that of the torque unit. Two coaxial hydraulic capsules separated by a common piston are rigidly attached to the motor casing or floating framework of the dynamometer. The liquid in these capsules is retained by rubber diaphragms in contact with the working surfaces of the piston. Pressure lines from both capsules are connected to a similar hydraulic capsule on a Toledo Printweigh scale to indicate the thrust. The thrust is proportional to the pressure difference of the liquid in the two capsules. In order to provide freedom of motion in the torque direction, the outer annular area of the thrust capsule piston is sandwiched between two air plates to make the piston float. The air plates are rigidly connected to the dynamometer barrel and contain high-pressure air chambers. The high-pressure air escapes from these chambers through small orifices and flows radially in both directions between the air plates and the piston. This air is exhausted through the main support strut. This thin film of air, 0.002 inch thick, transmits the load to be measured to the floating piston.

Since the air film between both thrust and torque air plates does not transmit shear loads, no interaction is possible between thrust and torque forces and cross calibrations have shown no interaction.

An 8-pole alternator is coupled to the shaft of one of the 200-horsepower motors and its output is fed into a frequency-measuring instrument to give the propeller revolutions per minute. A check on the accuracy of this instrument is provided by comparing its indicated frequency with a known Lissajous' figure on an oscilloscope; such checks give agreement to ±2 rpm through the whole speed range used in this investigation.

Thrust and torque calibrations of the dynamometer for each unit separately or for units coupled were the same and linear. Calibration curves are shown in figure 5 and the indicated thrust and torque loads are within ±0.25 percent of the applied loads for the range of loads of importance in this investigation. Periodic checks of the thrust and torque calibrations have shown no change in the calibrations.

APPENDIX B

PROPELLER THRUST

The tare thrust without the propeller is composed of skin friction D_{f_T} of the spinner and any change in thrust reaction $\Sigma \Delta p_T A$ produced by changes in pressure at the spinner gaps and inside the dynamometer, where A is the portion of the projected area of the floating part of the dynamometer affected by the pressure change Δp_T. Thus, the indicated tare thrust T_T becomes

$$T_T = D_{f_T} + \Sigma \Delta p_T A \tag{B1}$$

When the propeller is producing thrust, the indicated thrust is composed of the thrust T produced by the spinner-to-tip portion of the blade, spinner skin friction D_{f_P} and any change in thrust reaction $\Sigma \Delta p_P A$ produced by changes in pressure at the spinner gaps and inside the dynamometer. Thus the indicated propeller thrust, T_p, becomes

$$T_p = T + D_{f_P} + \Sigma \Delta p_P A \tag{B2}$$

and

$$T = T_P - D_{f_P} - \Sigma \Delta p_P A \tag{B3}$$

If the skin friction of the spinner is assumed to be the same with or without the propeller for the same conditions of tunnel and dynamometer operation, then D_{f_P} is equal to D_{f_T} and equation (B3) becomes

$$T = T_P - D_{f_T} - \Sigma \Delta p_P A \tag{B4}$$

The skin friction of the spinner as evaluated from the tare runs was found to be relatively independent of rotational speed and dependent on

tunnel Mach number only. Figure 8 shows the variation of measured skin friction with Mach number for this dynamometer. The theoretical skin friction calculated for a flat plate based on a turbulent boundary layer and the local Reynolds number (reference 6) is shown for comparison. The agreement is good.

It was necessary to measure pressures at nine locations in the dynamometer housing and at three radial locations on each side of the spinner in order to evaluate the changes in thrust produced by changes in pressure. The locations at which pressure measurement were made are shown in figure 1. The complete system was checked to insure correct evaluation of thrust changes due to pressure by applying known internal pressures throughout the dynamometer barrel. Checks of this were made frequently for the dynamometer without a propeller, and the change in indicated thrust checked the calculated change due to pressure within ±0.15 pound.

Very little change in spinner-gap pressure was measured when the shank sections of the propeller were unstalled or operating at subcritical speeds. Larger changes in pressure occurred, however, at both the front and rear gaps of the spinner for supercritical shank section operation amounting to 13 percent of the propeller thrust at a Mach number of 0.925 for $\beta_{0.75R} = 55^\circ$ and as much as 100 percent of the propeller thrust at a Mach number of 0.925 for $\beta_{0.75R} = 70^\circ$. This was for maximum-efficiency operation of the propeller. Very little change in pressure was measured at the nine locations inside the dynamometer. These changes show that, for propeller testing at high forward speeds, particular care must be given to pressure instrumentation in order to insure accurate evaluation of propeller thrust.

REFERENCES

1. Carmel, Melvin M., and Robinson, Harold L.: Further Investigation of NACA 4-(5)(08)-03 Two-Blade Propeller at High Forward Speeds. NACA RM L7E12, 1947.

2. Delano, James B.: Investigation of Two-Blade Propellers at High Forward Speeds in the NACA 8-Foot High-Speed Tunnel. III - Effects of Camber and Compressibility. NACA 4-(5)(08)-03 and NACA 4-(10)(08)-03 Blades. NACA ACR L5F14, 1945.

3. Fage, A., Lock, C. N. H., Bateman, H., and Williams, D. H.: Experiments with a Family of Airscrews Including Effect of Tractor and Pusher Bodies. Part II - Experiments on Airscrews with Tractor and Pusher Bodies. R. & M. No. 830, British A.R.C., 1922.

4. Glauert, H.: The Elements of Aerofoil and Airscrew Theory. American ed., The Macmillan Co., 1943, pp. 222-226.

5. Young, A. D.: Note on the Application of the Linear Perturbation Theory to Determine the Effect of Compressibility on the Wind Tunnel Constraint on a Propeller. RAE TN No. Aero. 1539, Nov. 1944.

6. Von Mises, Richard: The Theory of Flight. McGraw-Hill Book Co., Inc., 1945, p. 106.

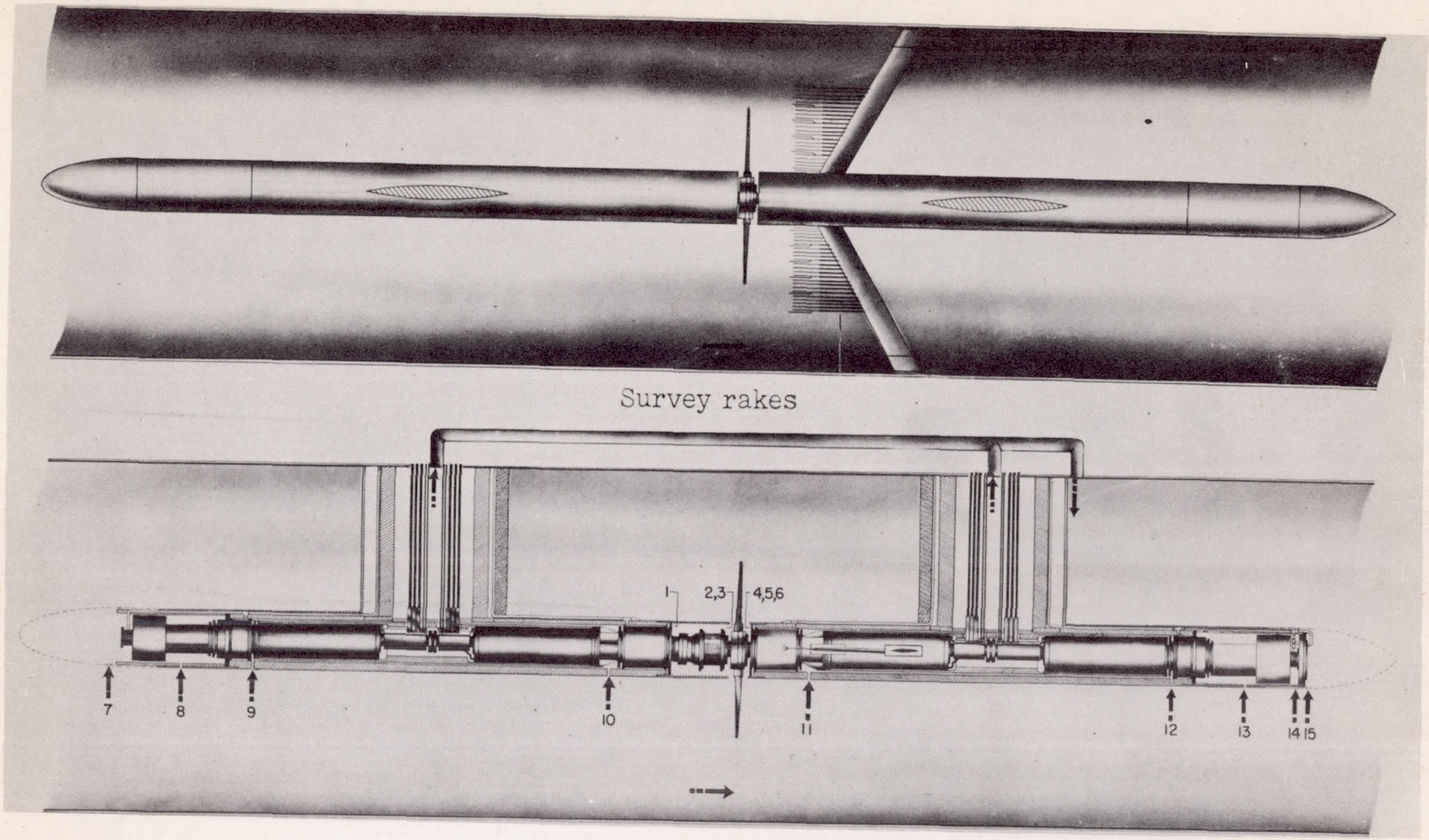

NACA

L-61063

Figure 1.- Installation of propeller dynamometer in Langley 8-foot high-speed tunnel.

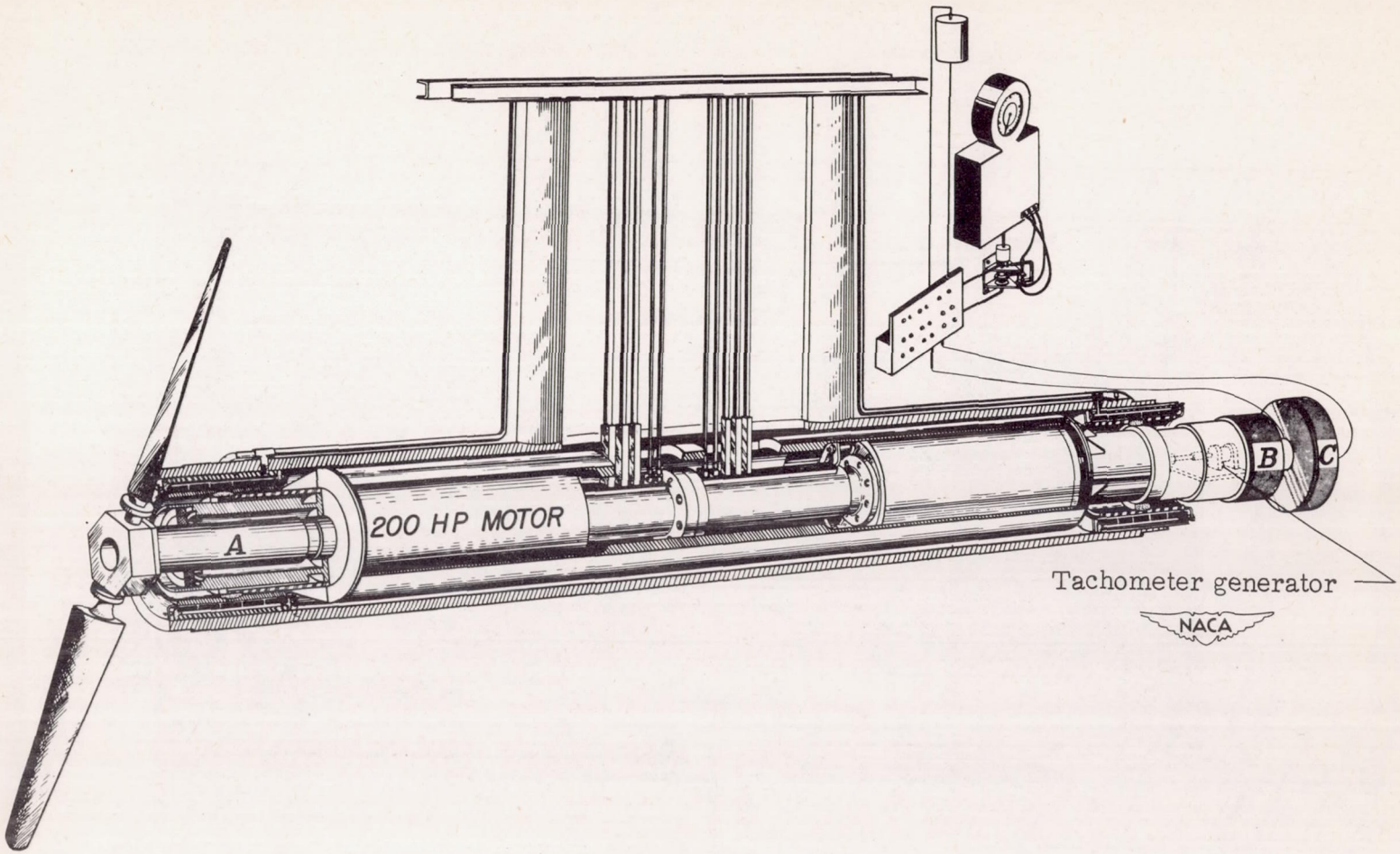

(a) Cross-sectional view of one unit.

Figure 2.- Views showing dynamometer details.

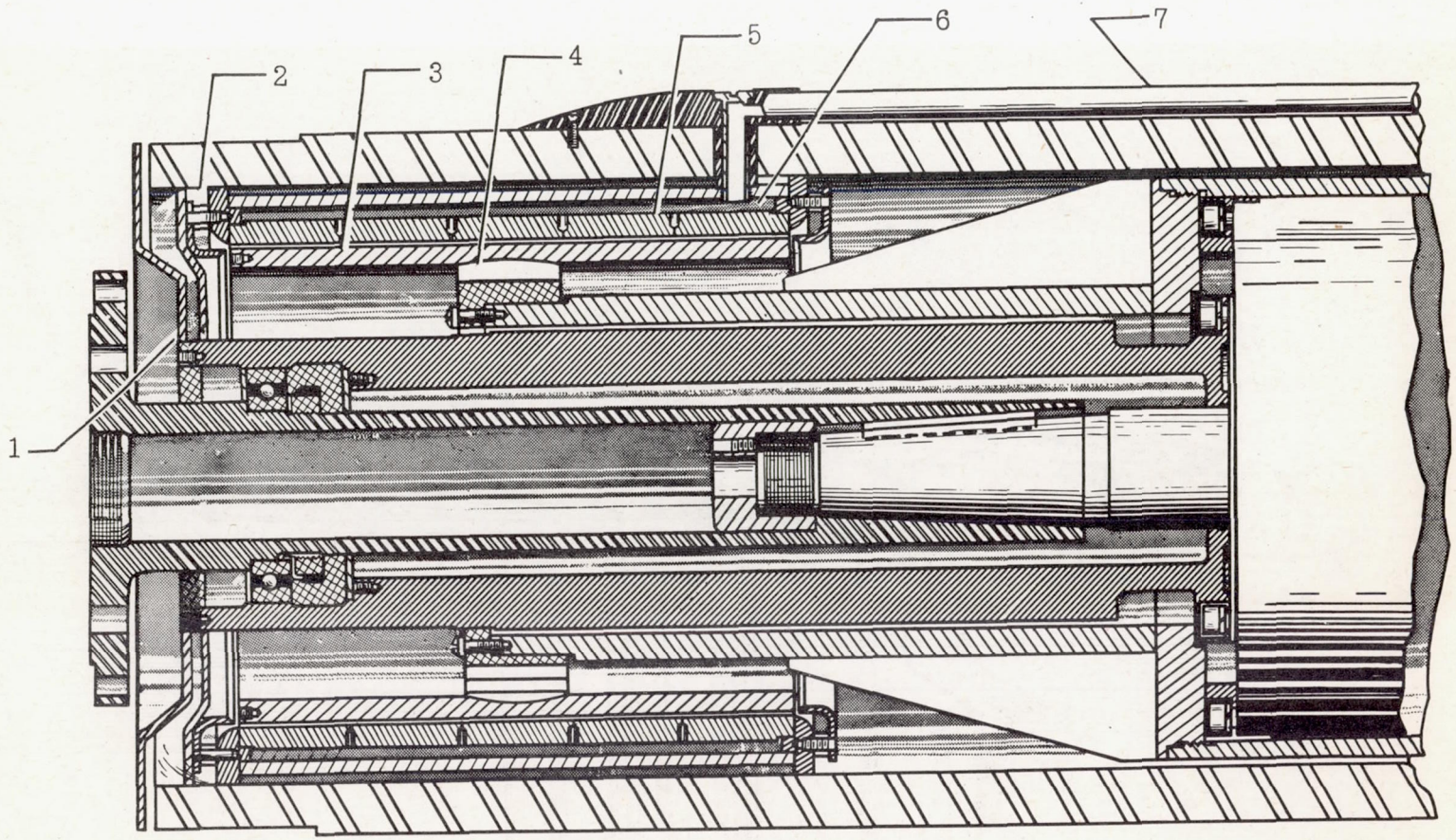

Detail A. Floating bearing unit

1. Labyrinth seal
2. Exhaust air
3. Bearing floating sleeve
4. Alinement ring
5. Air bearing
6. Air chamber
7. Air pressure

NACA

(b) Floating-bearing unit.

Figure 2.- Continued.

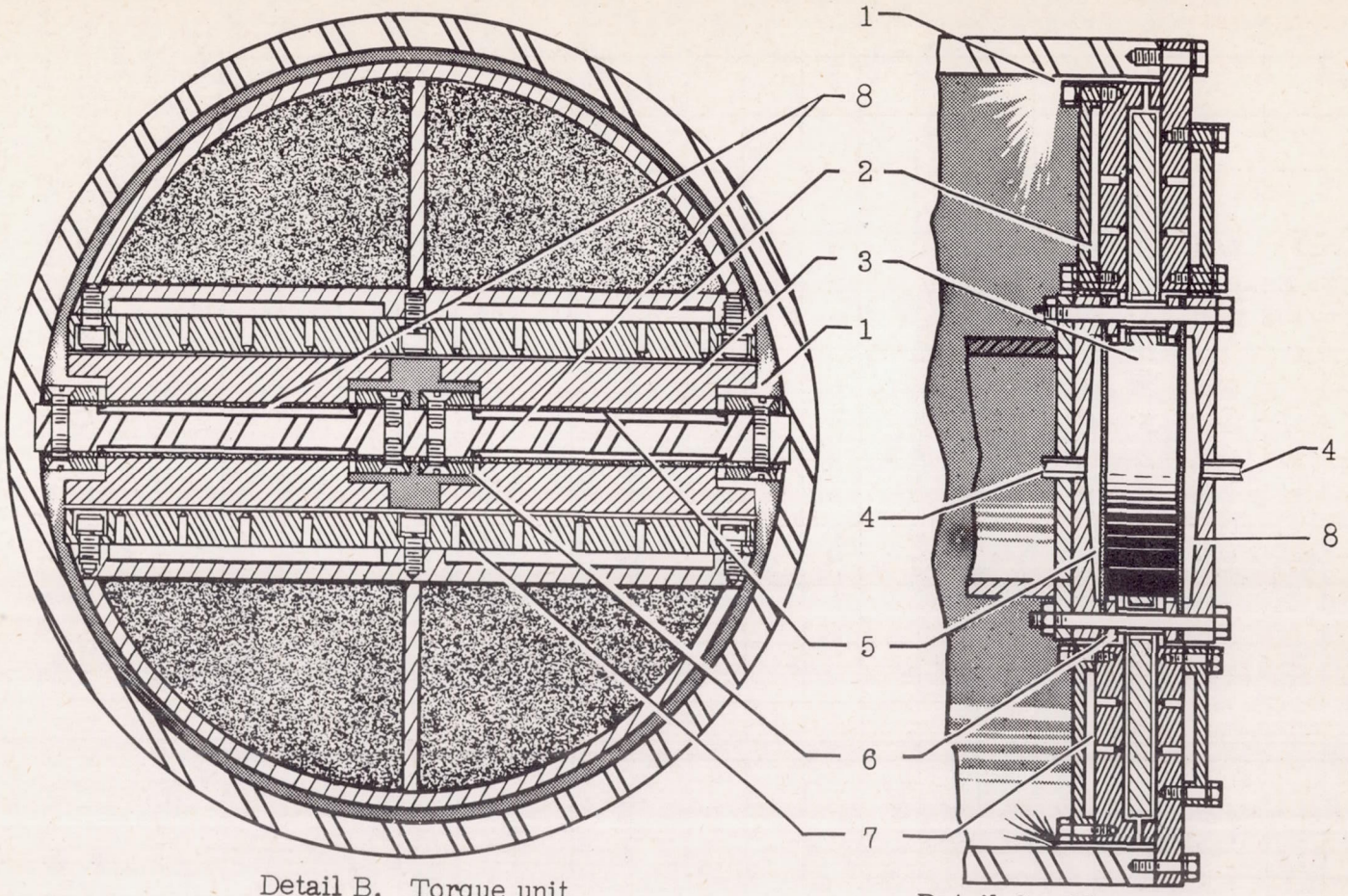

Detail B. Torque unit

Detail C. Thrust unit

1. Exhaust air
2. Air chamber
3. Floating piston
4. Pressure leads
5. Diaphragm
6. Diaphragm clamping ring
7. Air plates
8. Constant pressure cell

(c) Torque and thrust units.

Figure 2.– Concluded.

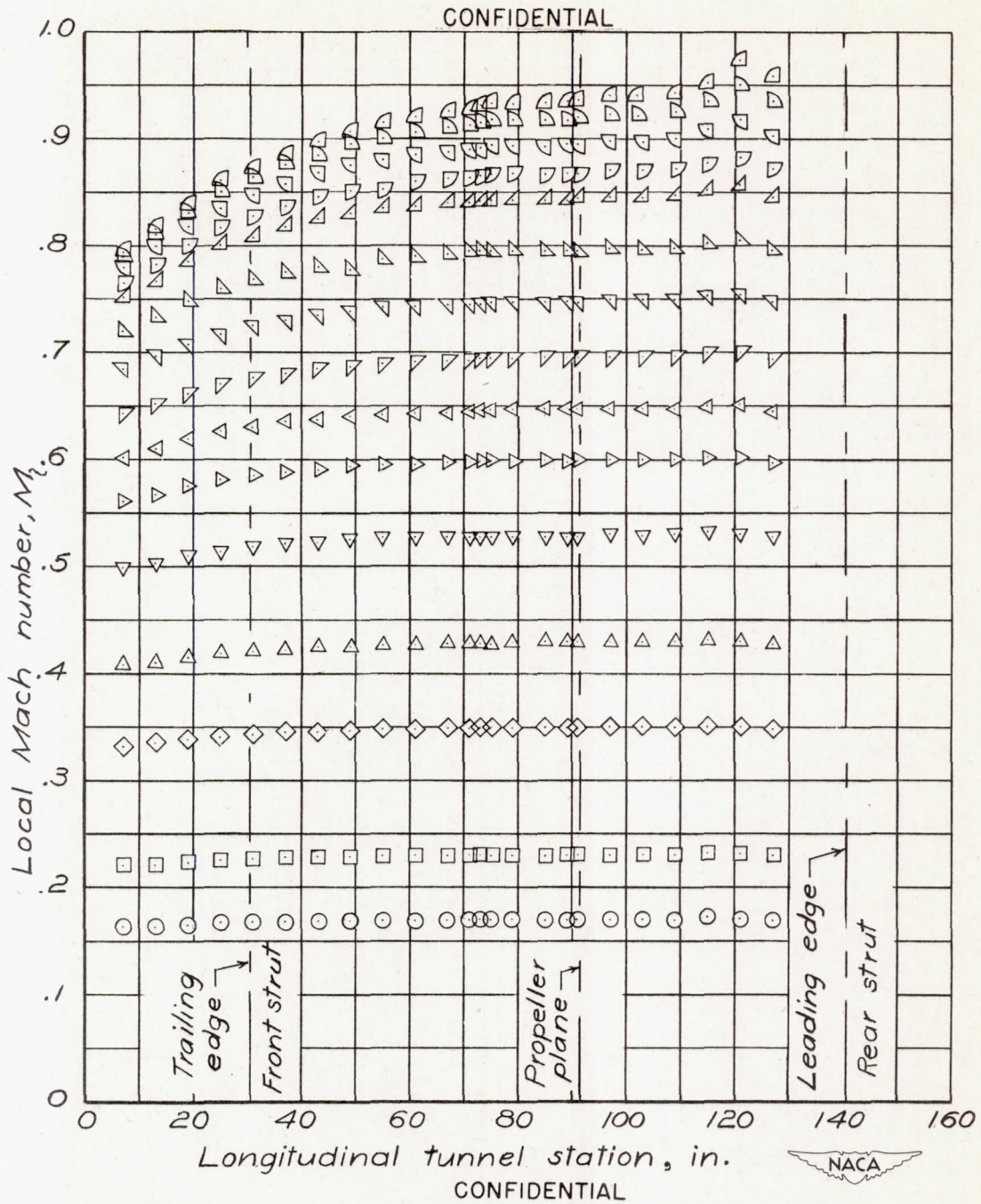

Figure 3.- Longitudinal Mach number distribution in the Langley 8-foot high-speed tunnel 18 inches below the surface of the dynamometer without propeller.

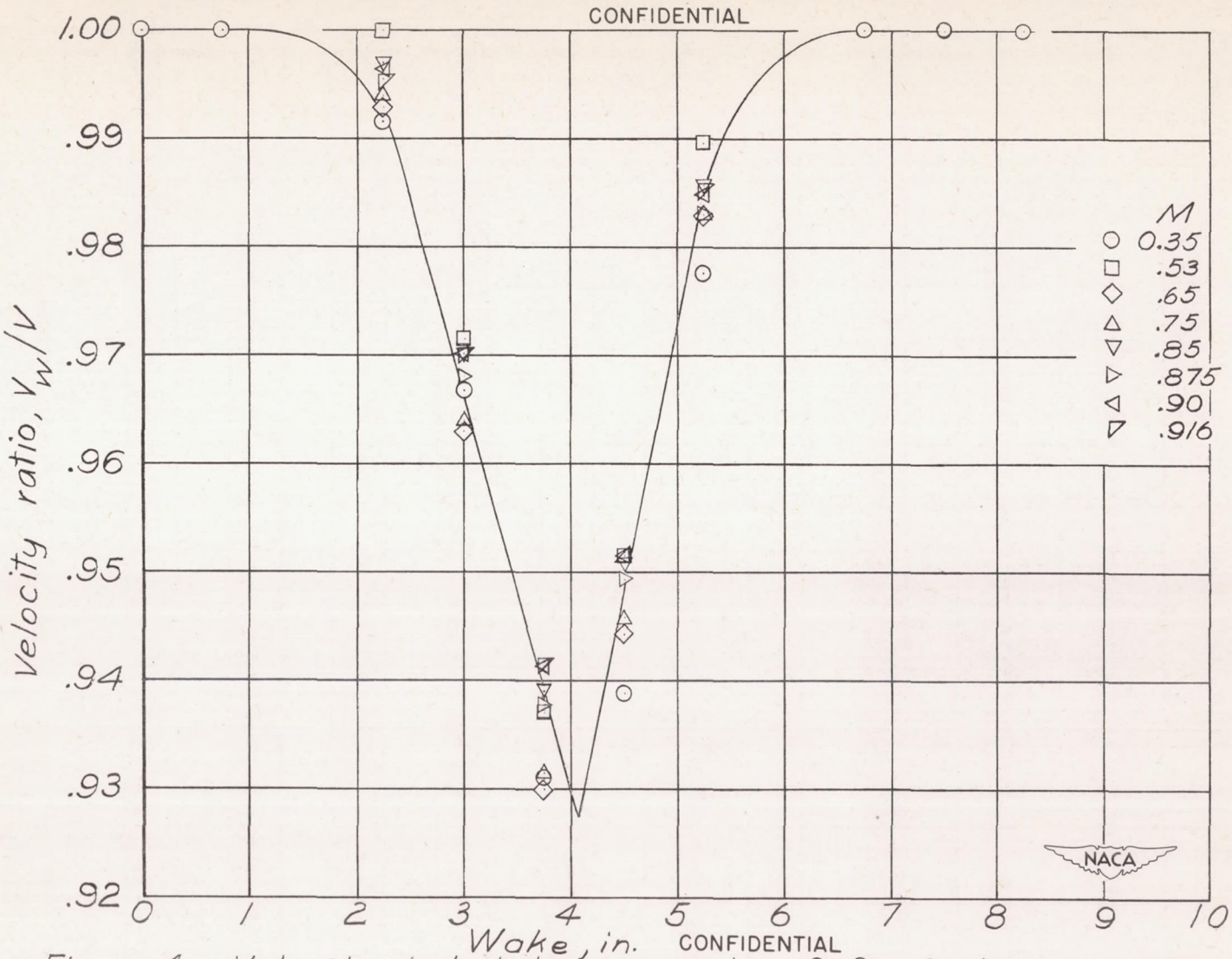

Figure 4.- Velocity distribution in wake of front-dynamometer support strut.

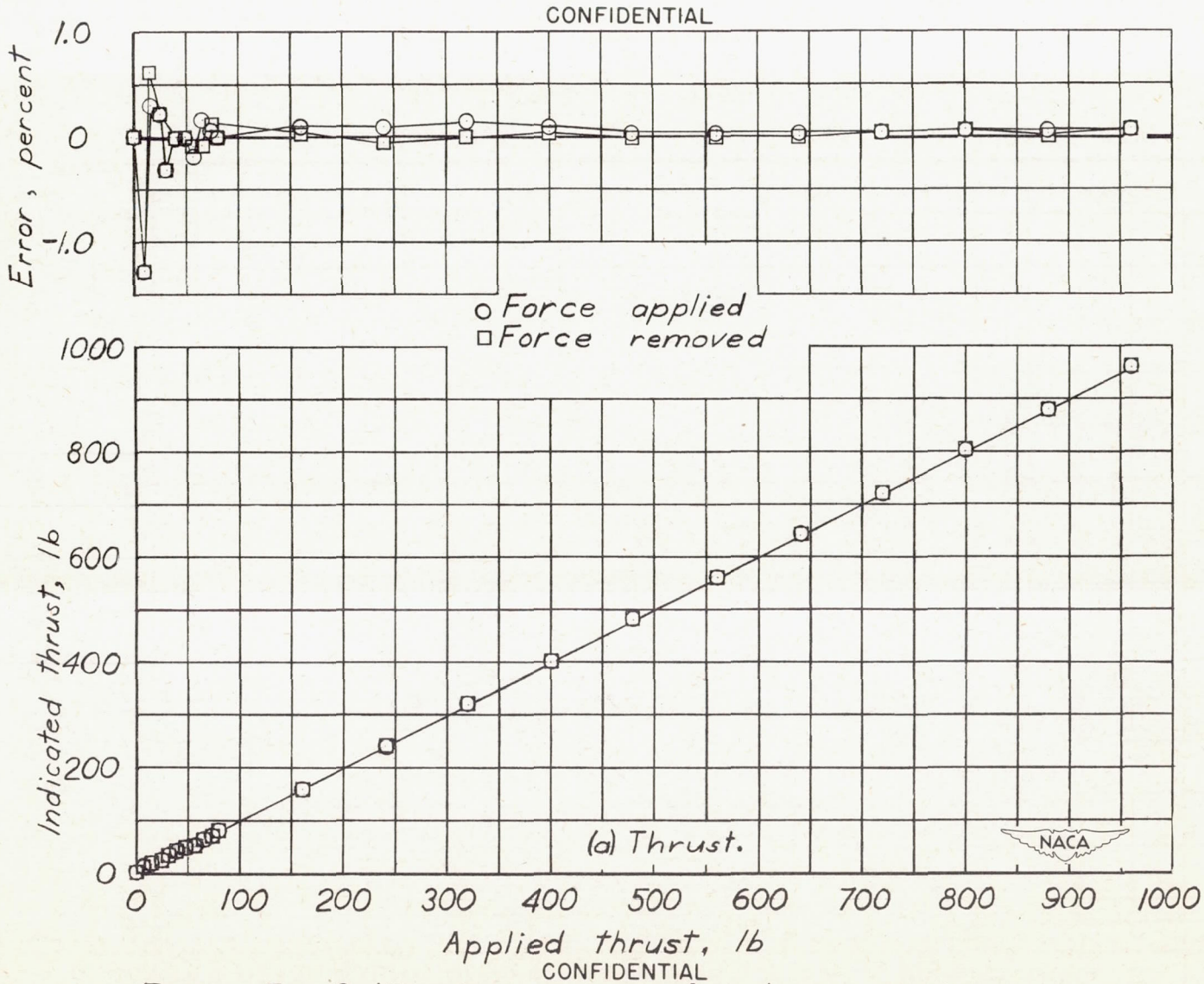

Figure 5.- Calibration curves for dynamometer.

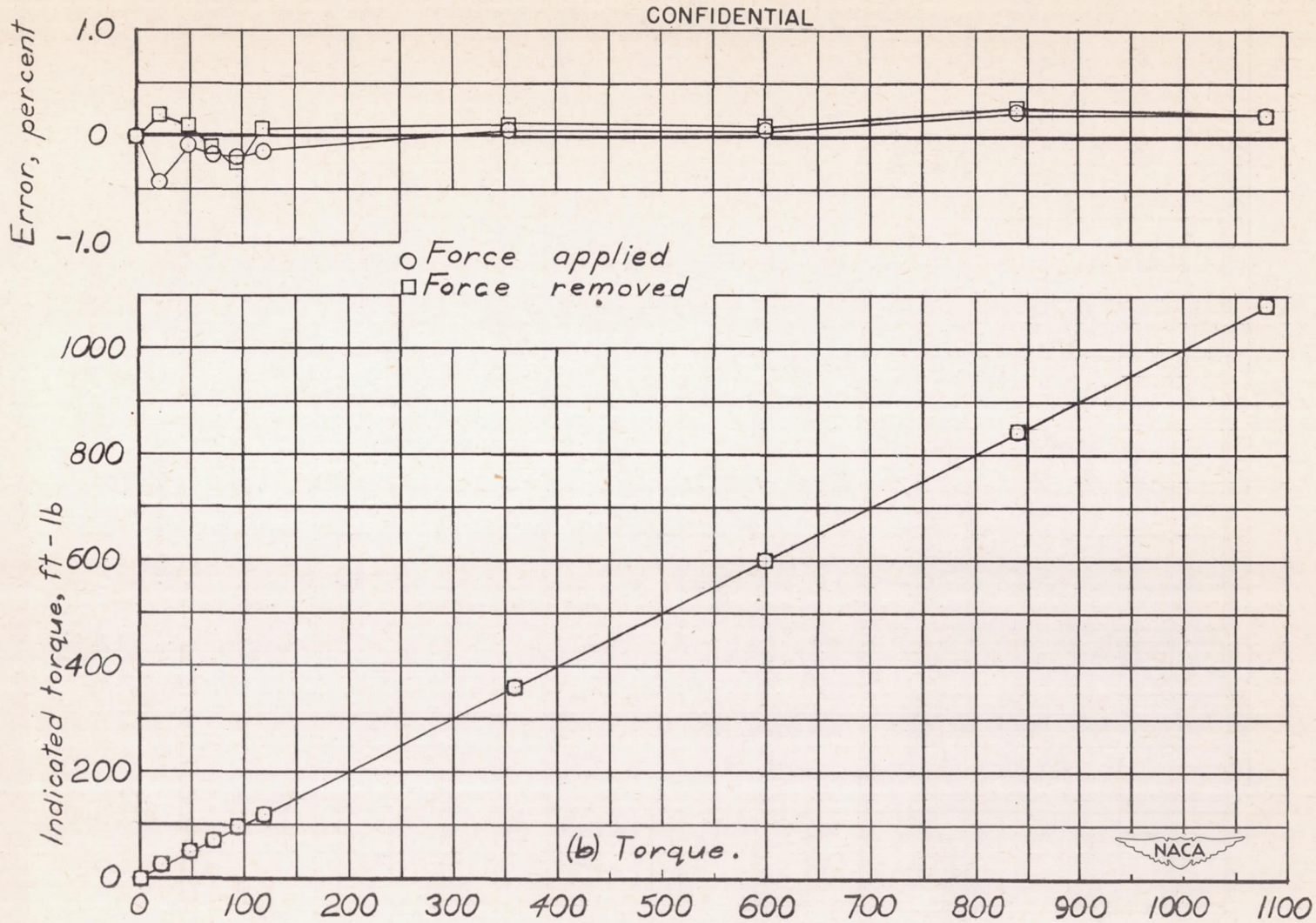

Figure 5.-Concluded.

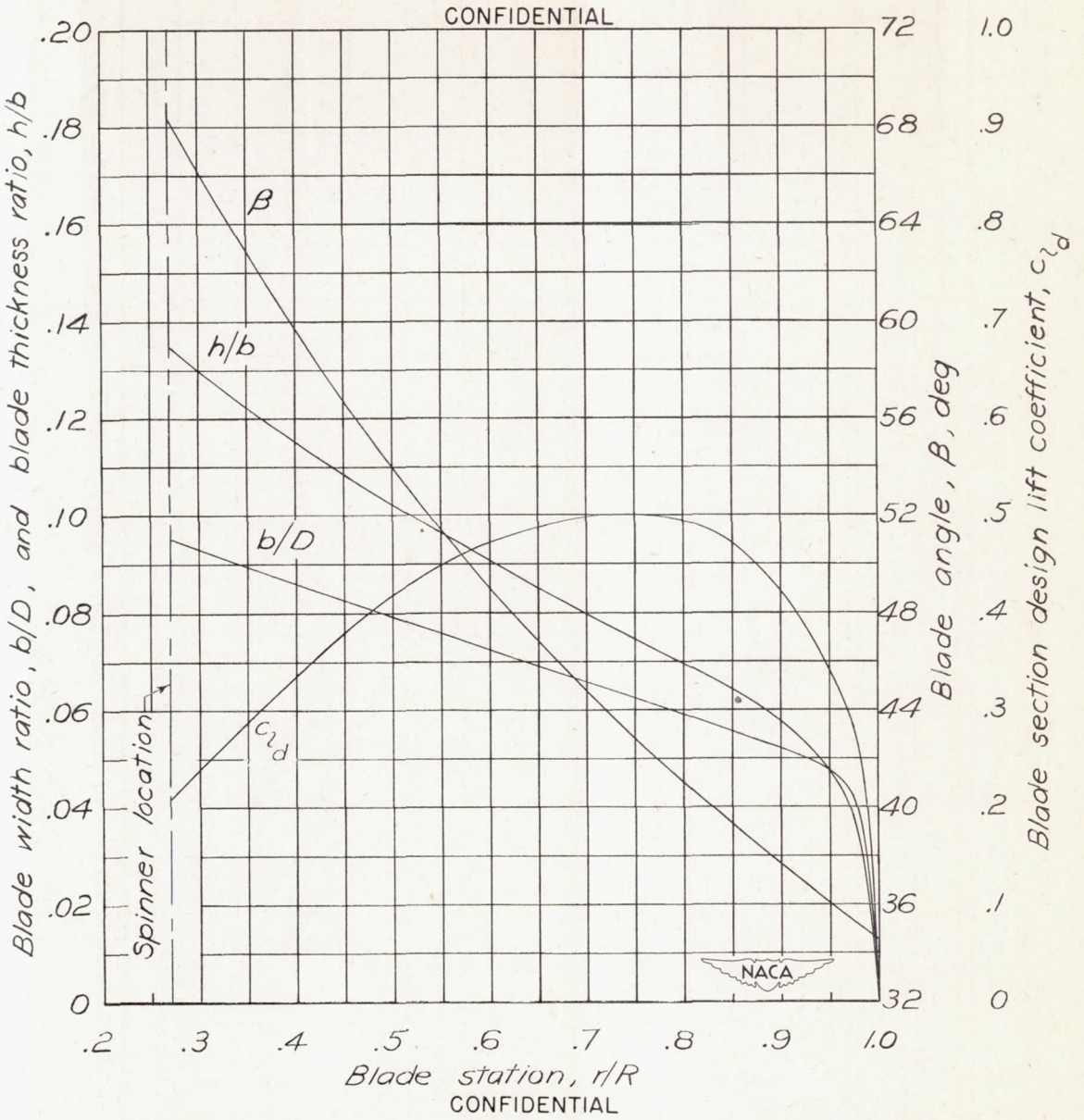

Figure 6.- NACA 4-(5)(08)-03 propeller-blade-form curves.

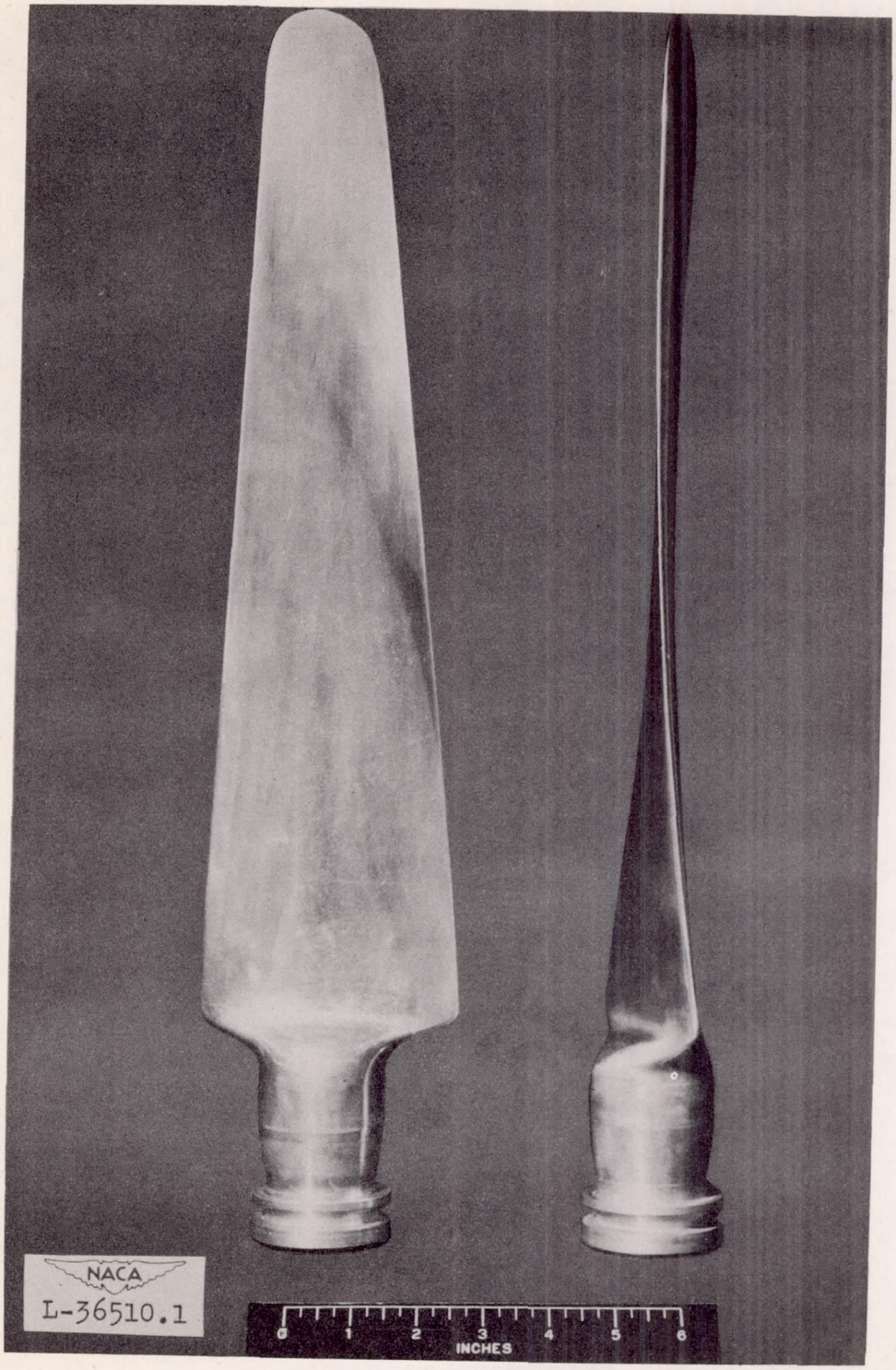

Figure 7.- Photograph of NACA 4-(5)(08)-03 propeller.

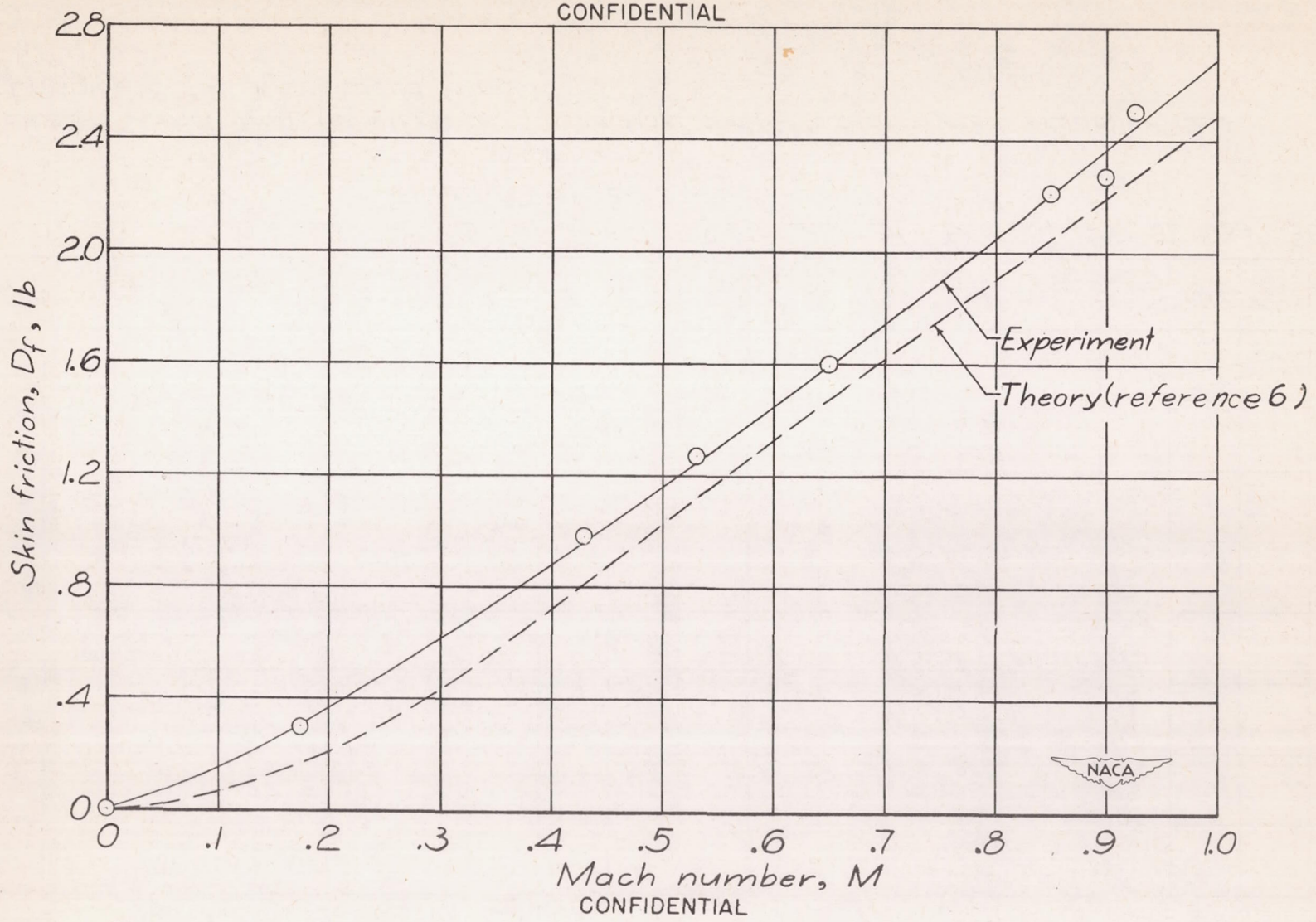

Figure 8.- Propeller-spinner skin friction.

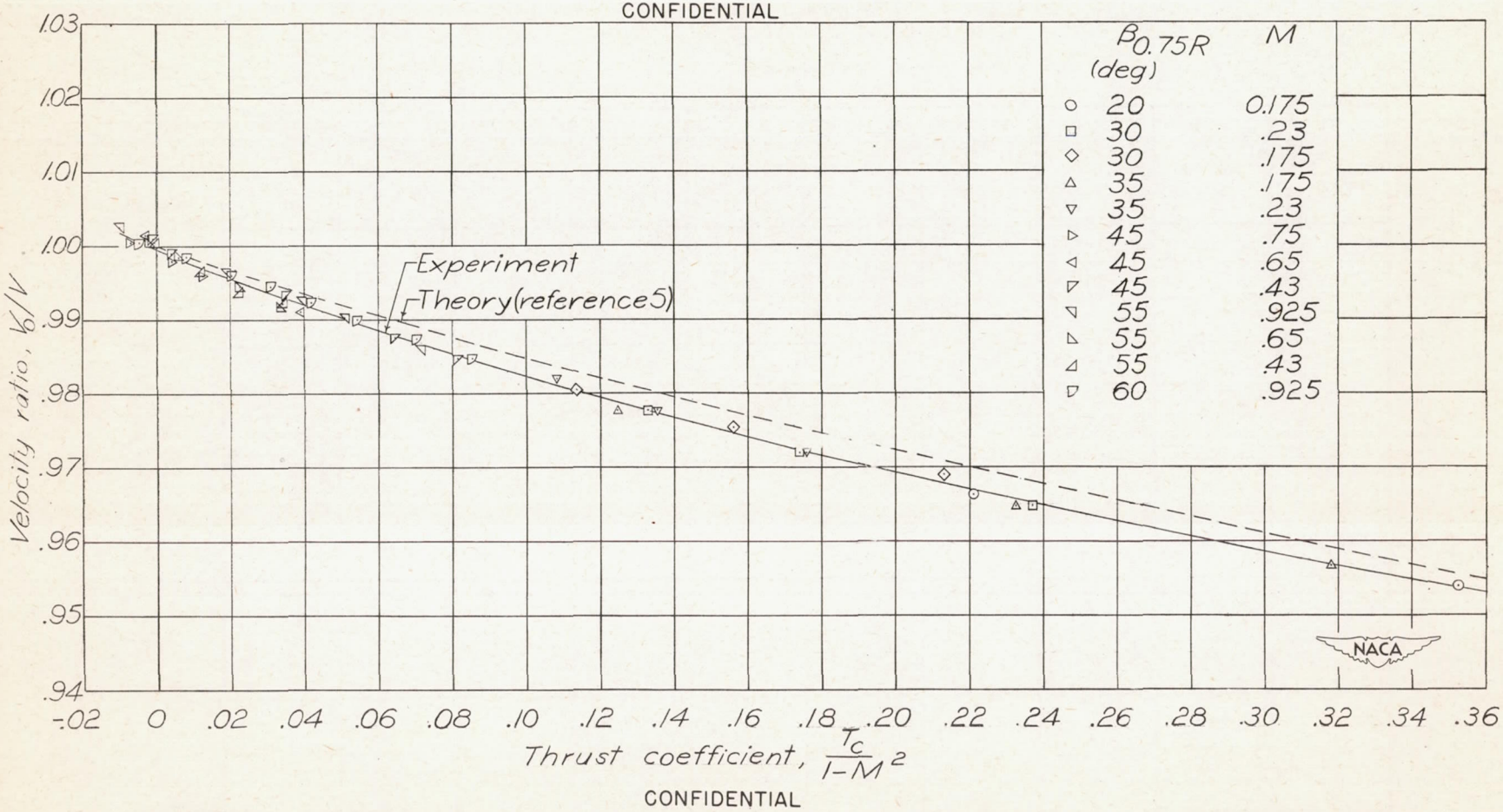

Figure 9.- Tunnel-wall-interference correction for 4-foot-diameter propeller in Langley 8-foot high-speed tunnel.

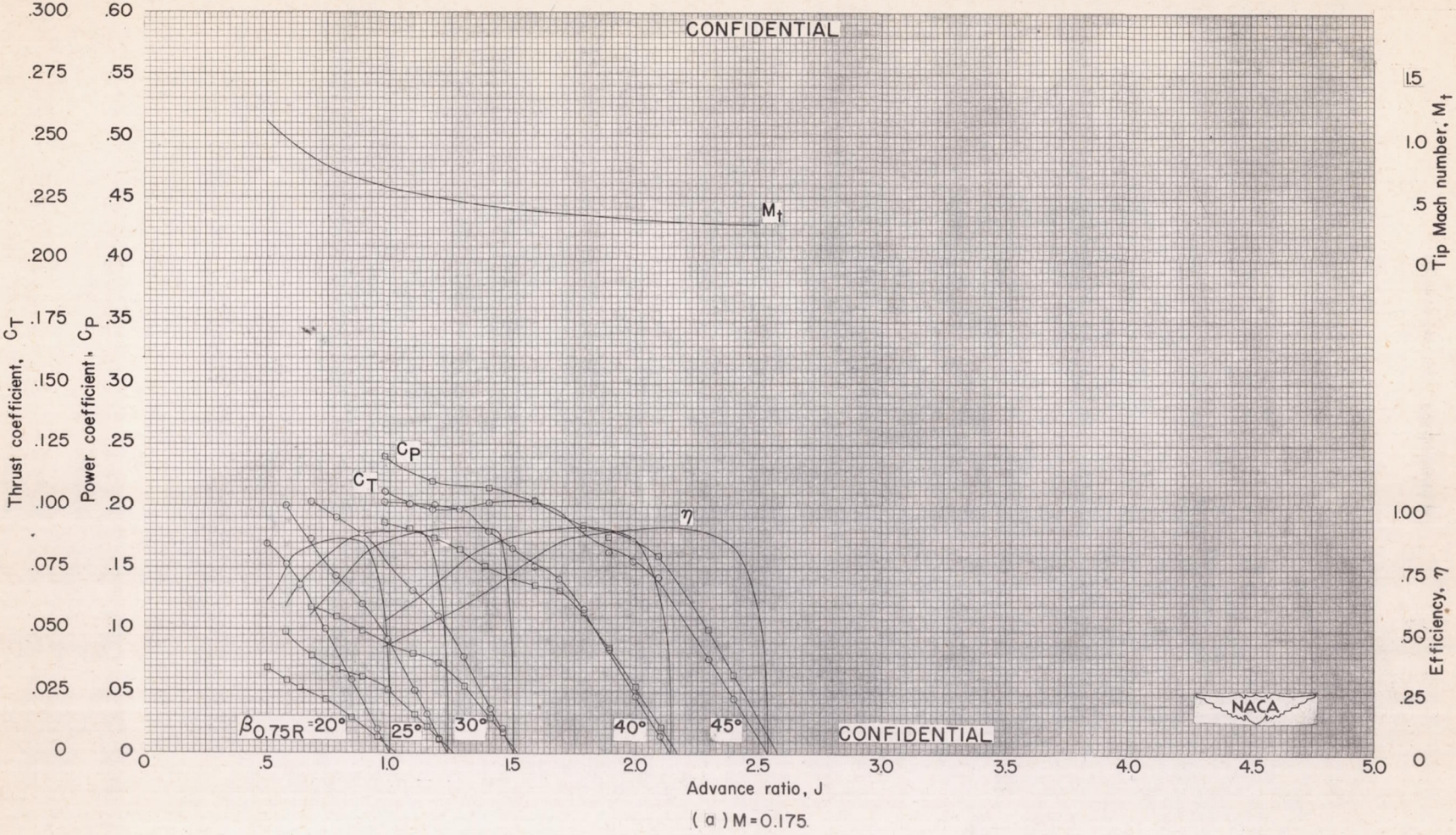

Figure 10 .- Characteristics of NACA propeller 4-(5)(08)-03.

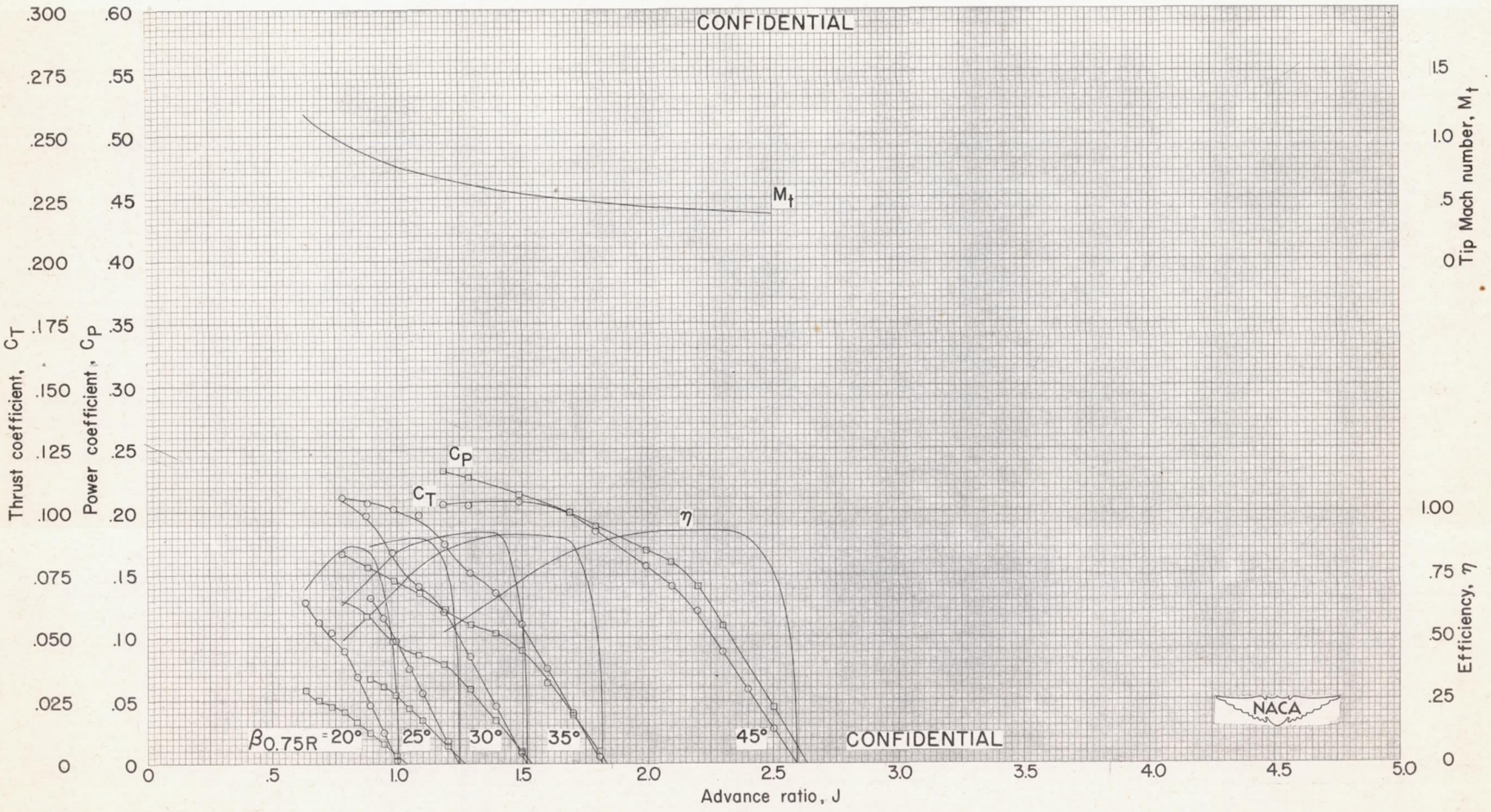

(b) M=0.23.

Figure 10 - Continued.

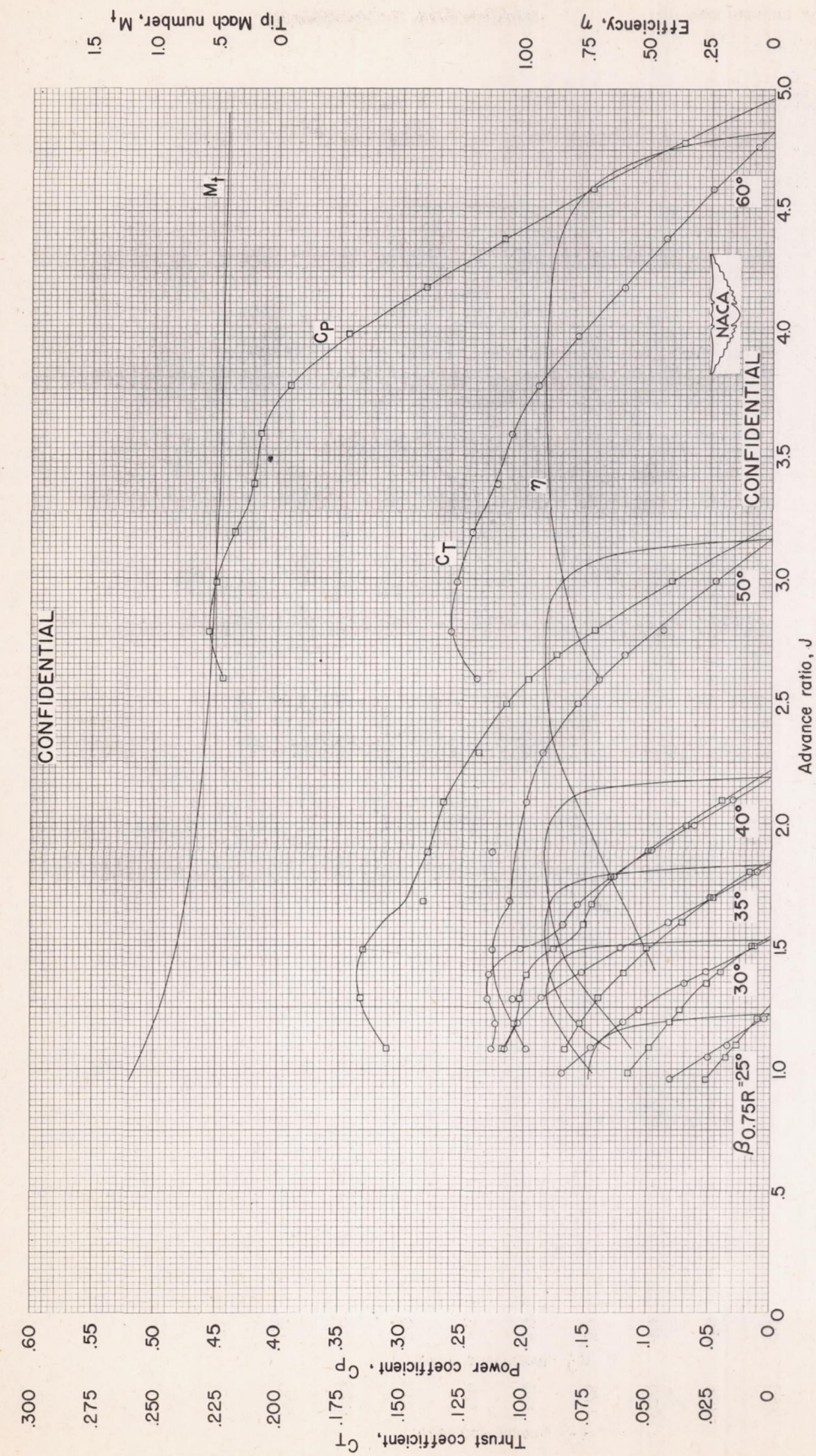

(c) M=0.35.

Figure 10 - Continued.

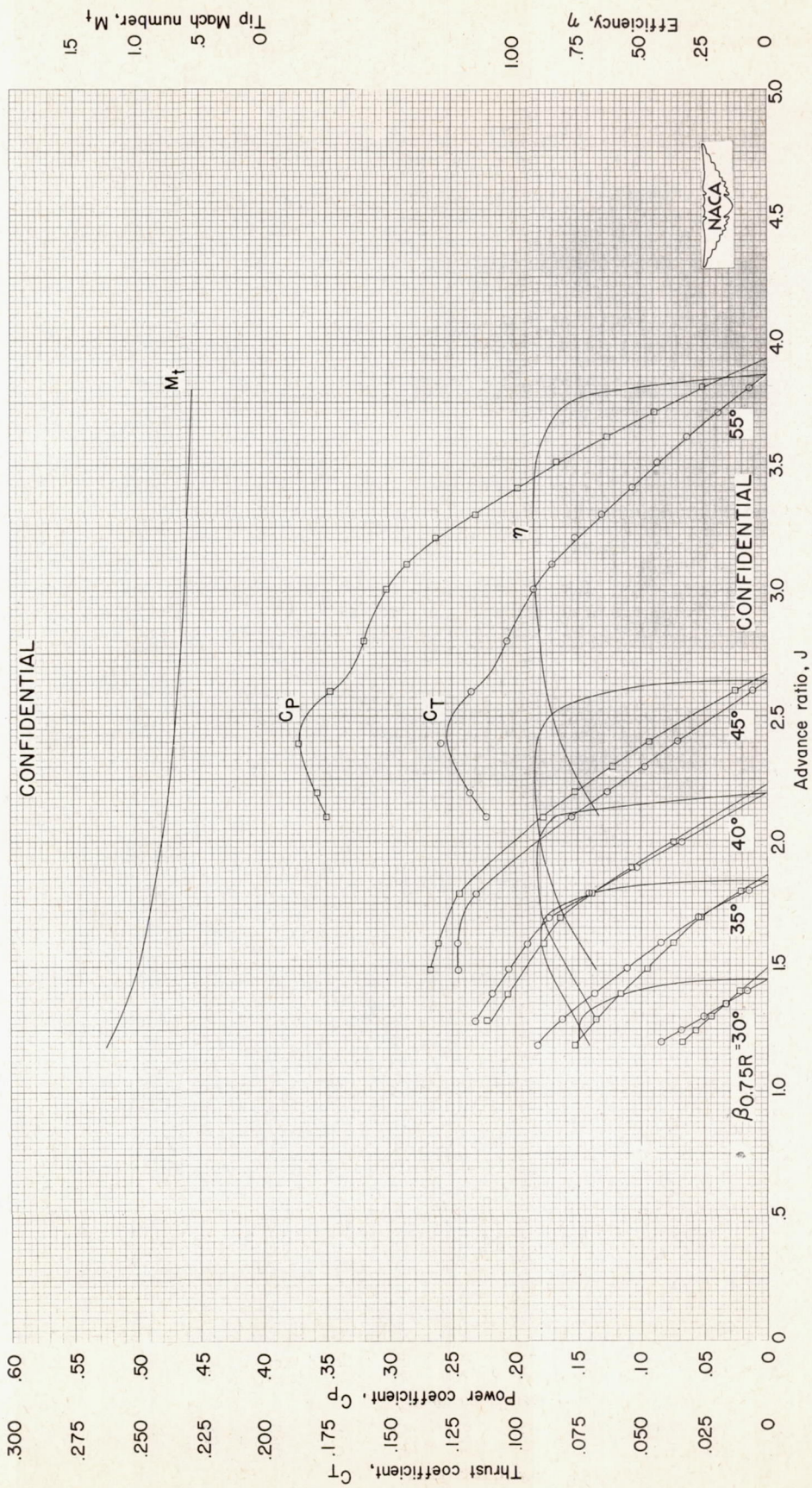

Figure 10 - Continued.

(d) M=0.43.

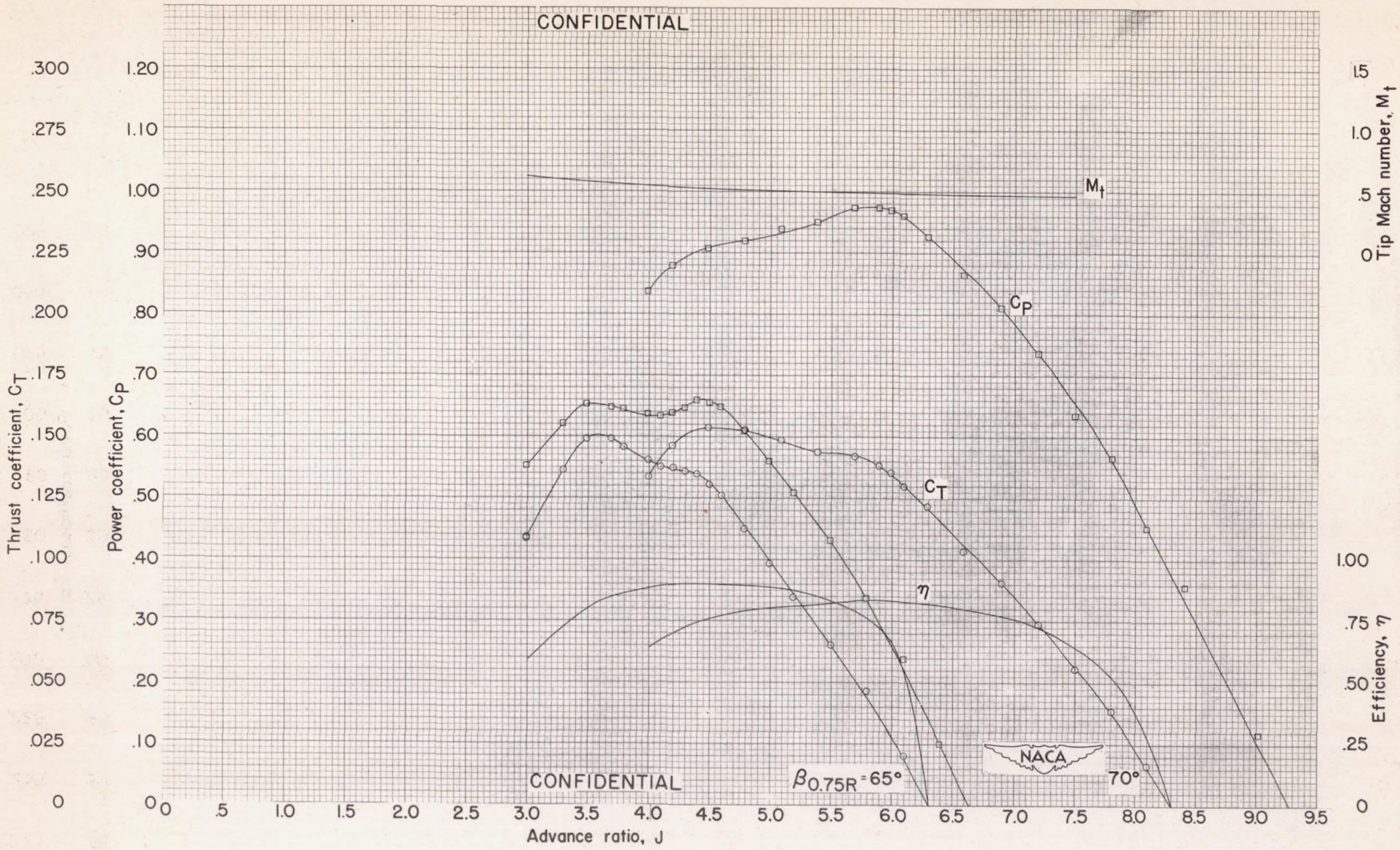

(d) M=0.43. Concluded.

Figure 10 - Continued.

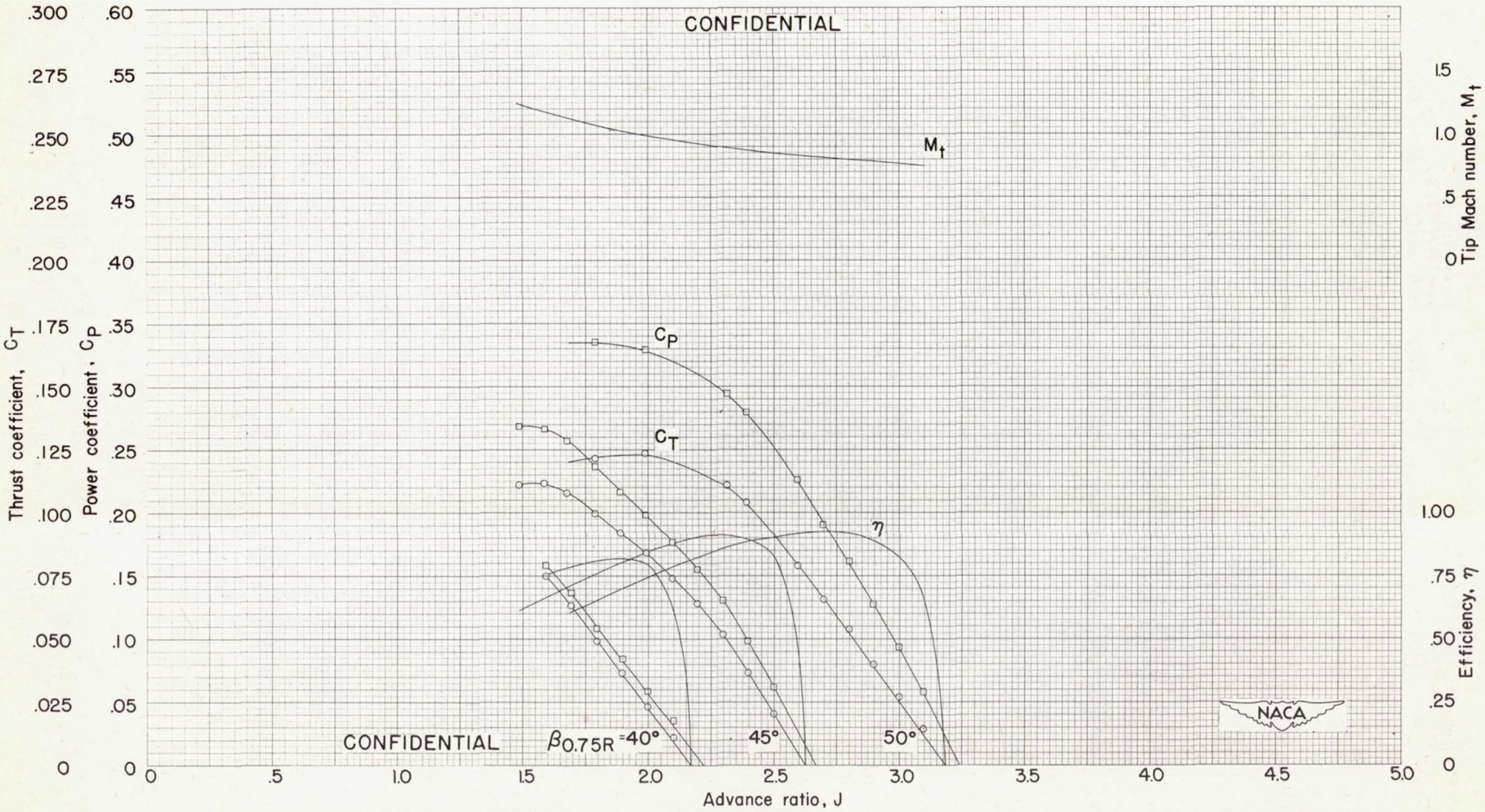

(e) M=0.53.

Figure 10 - Continued.

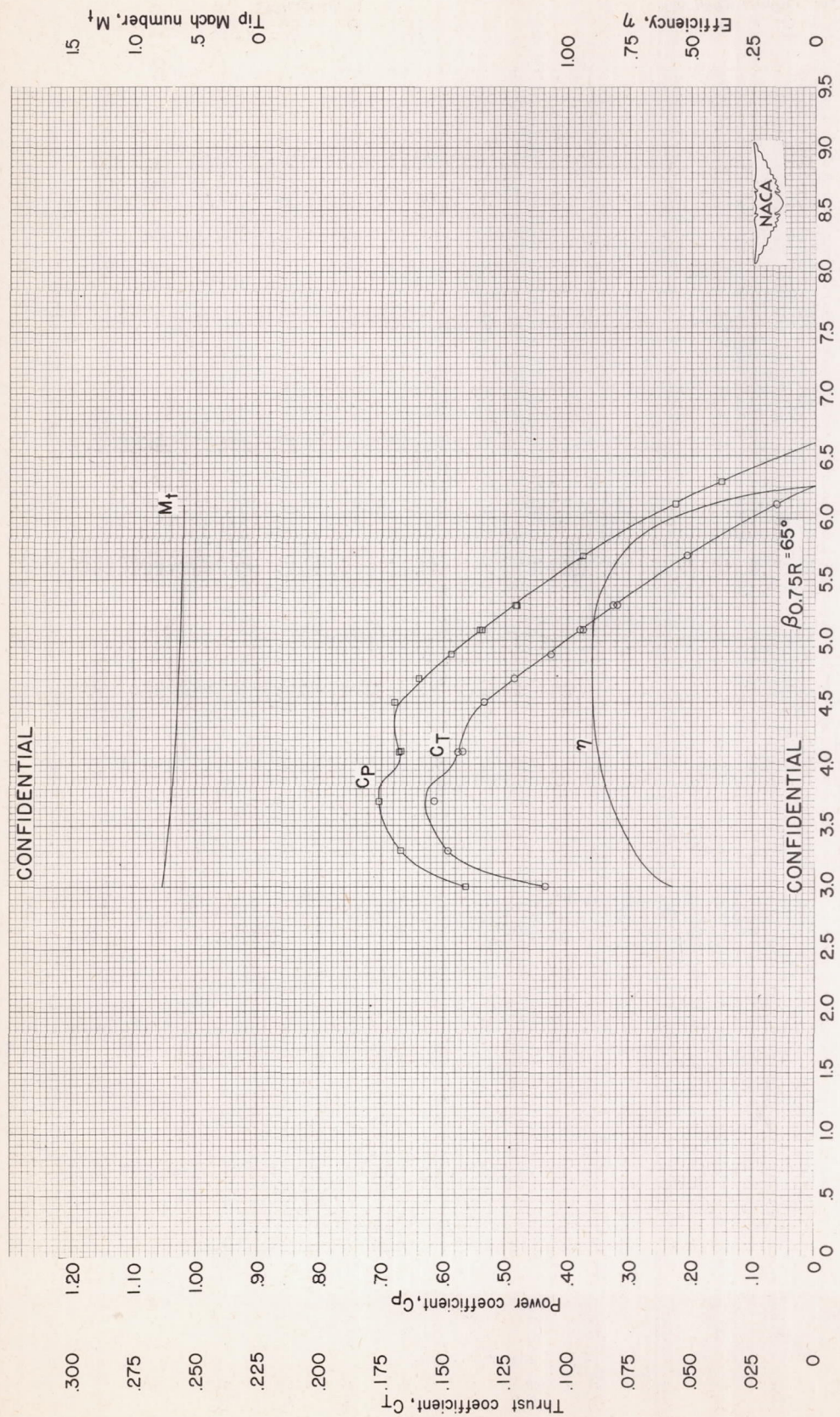

(e) M=0.53 Concluded.

Figure 10 - Continued.

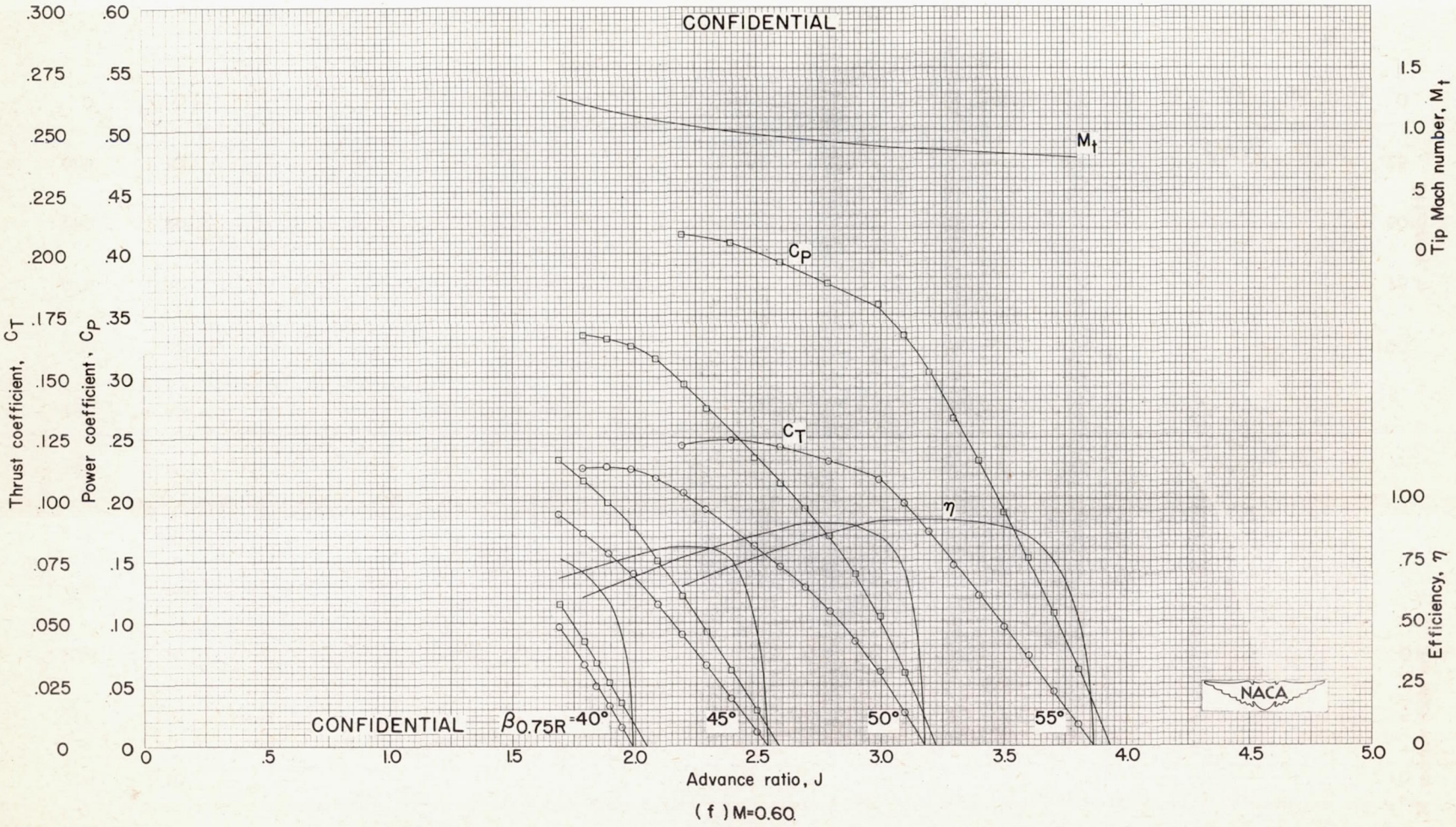

(f) M=0.60

Figure 10 - Continued.

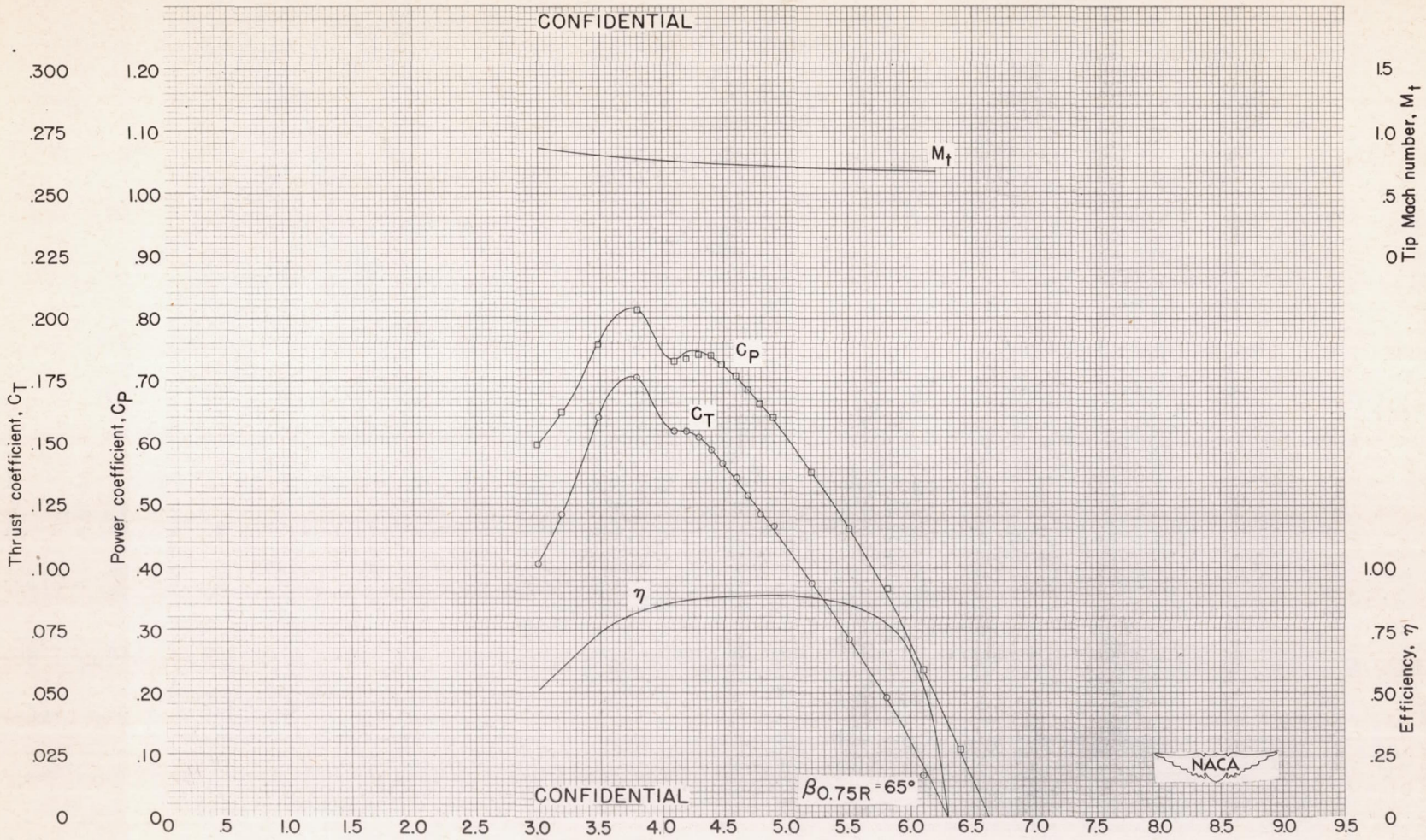

(f) M=0.60. Concluded.

Figure 10 - Continued.

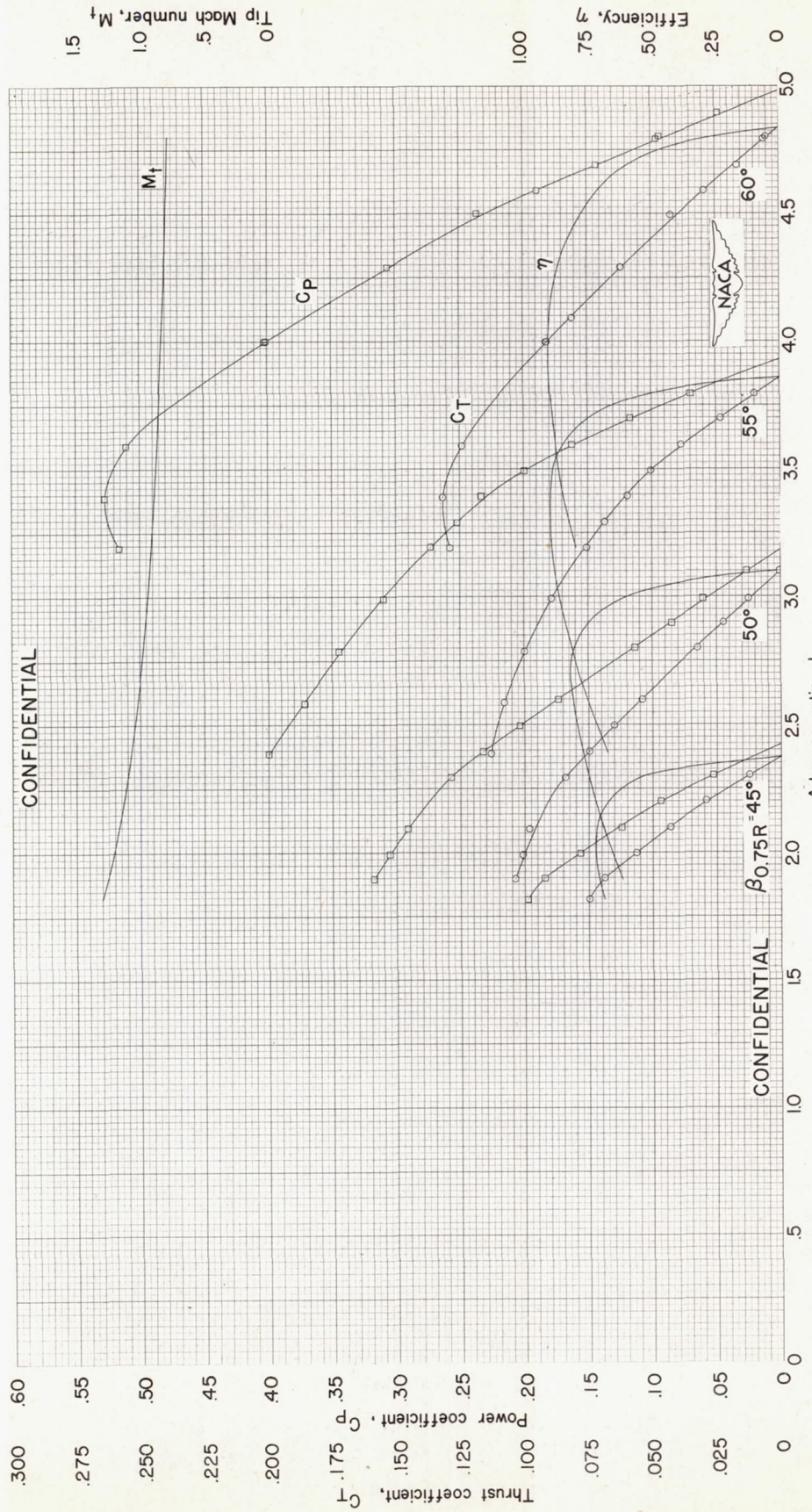

Figure 10 - Continued.

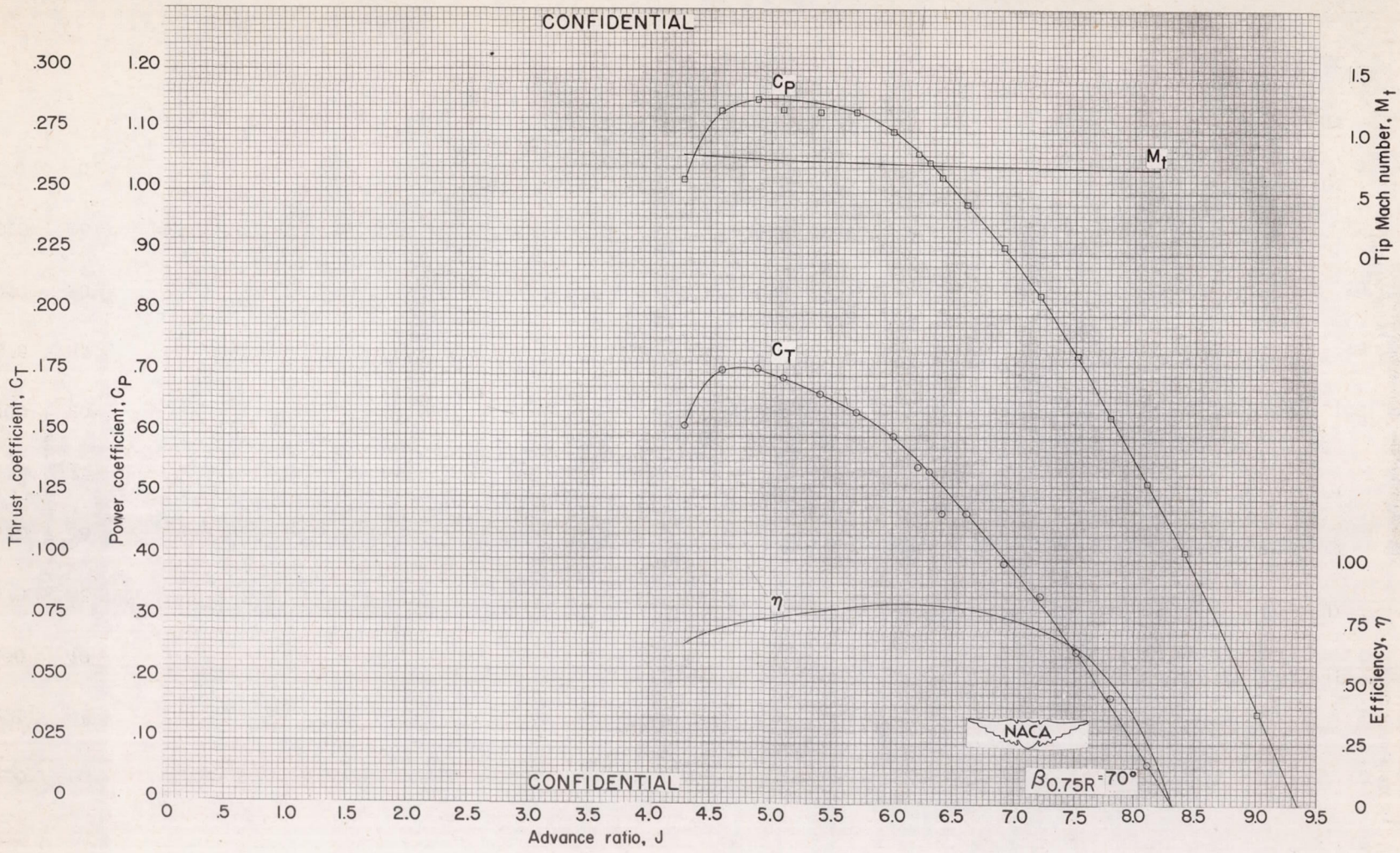

(g) M=0.65. Concluded.

Figure 10 - Continued.

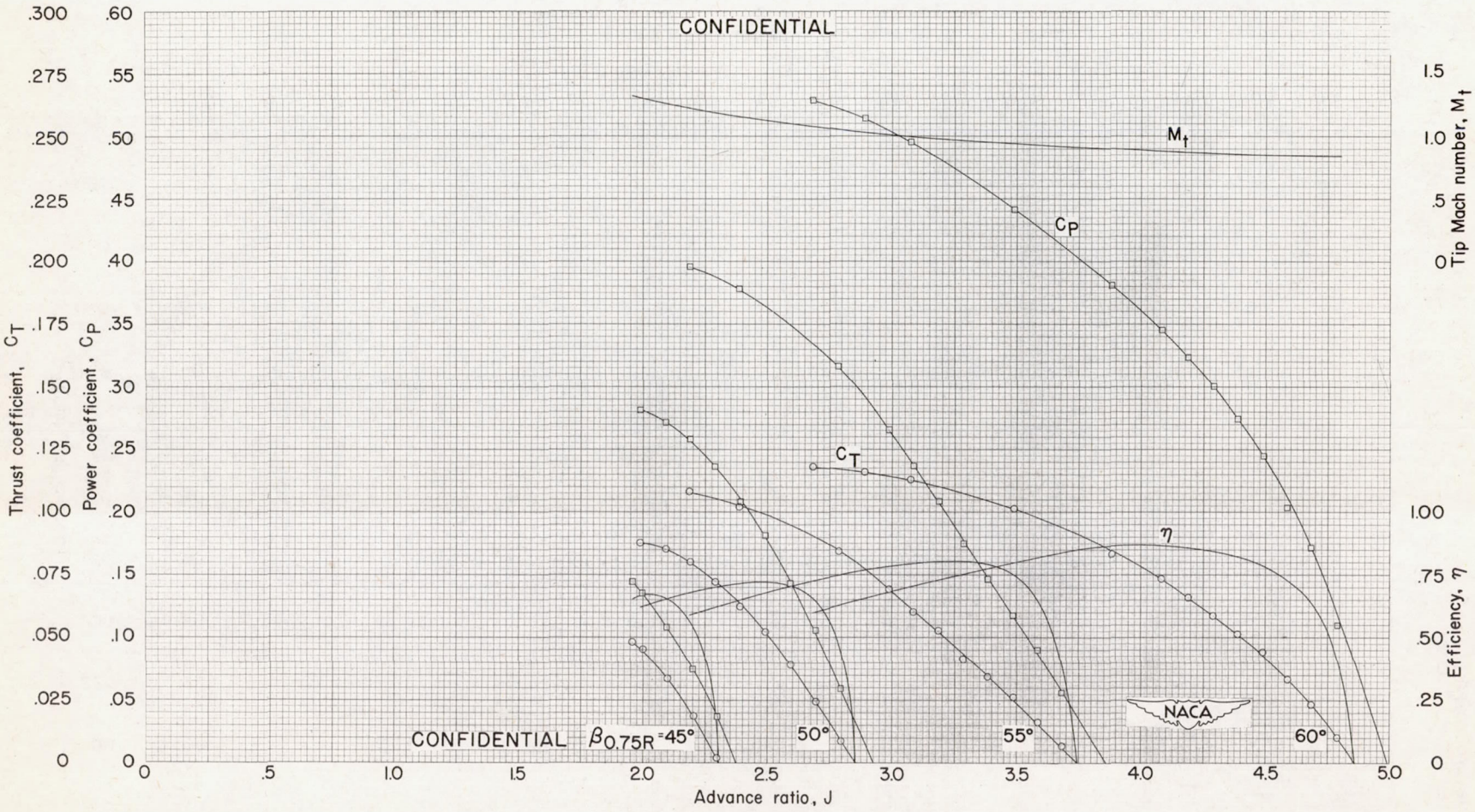

(h) M=0.70.

Figure 10 .- Continued.

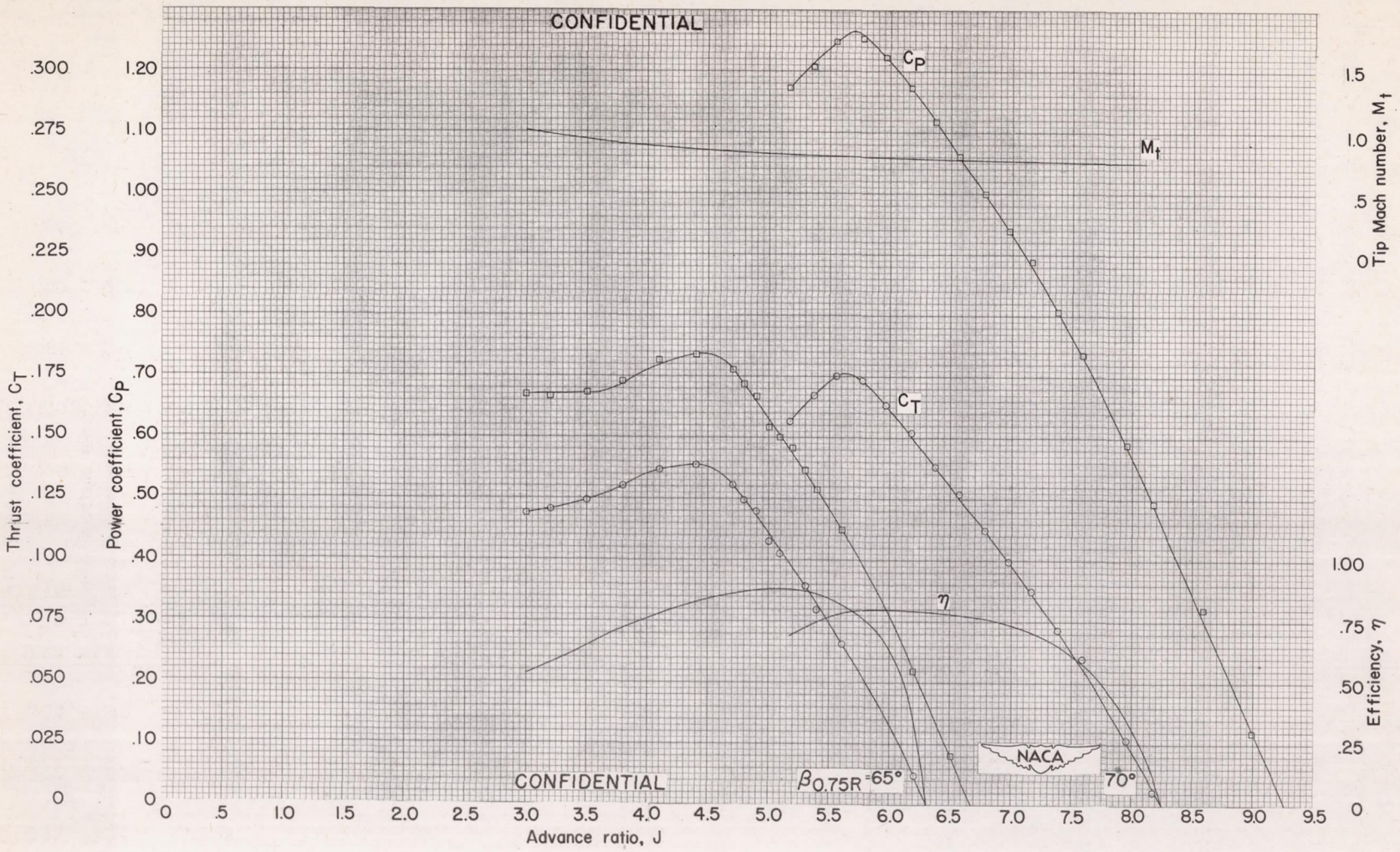

(h) M=0.70. Concluded.

Figure 10 - Continued.

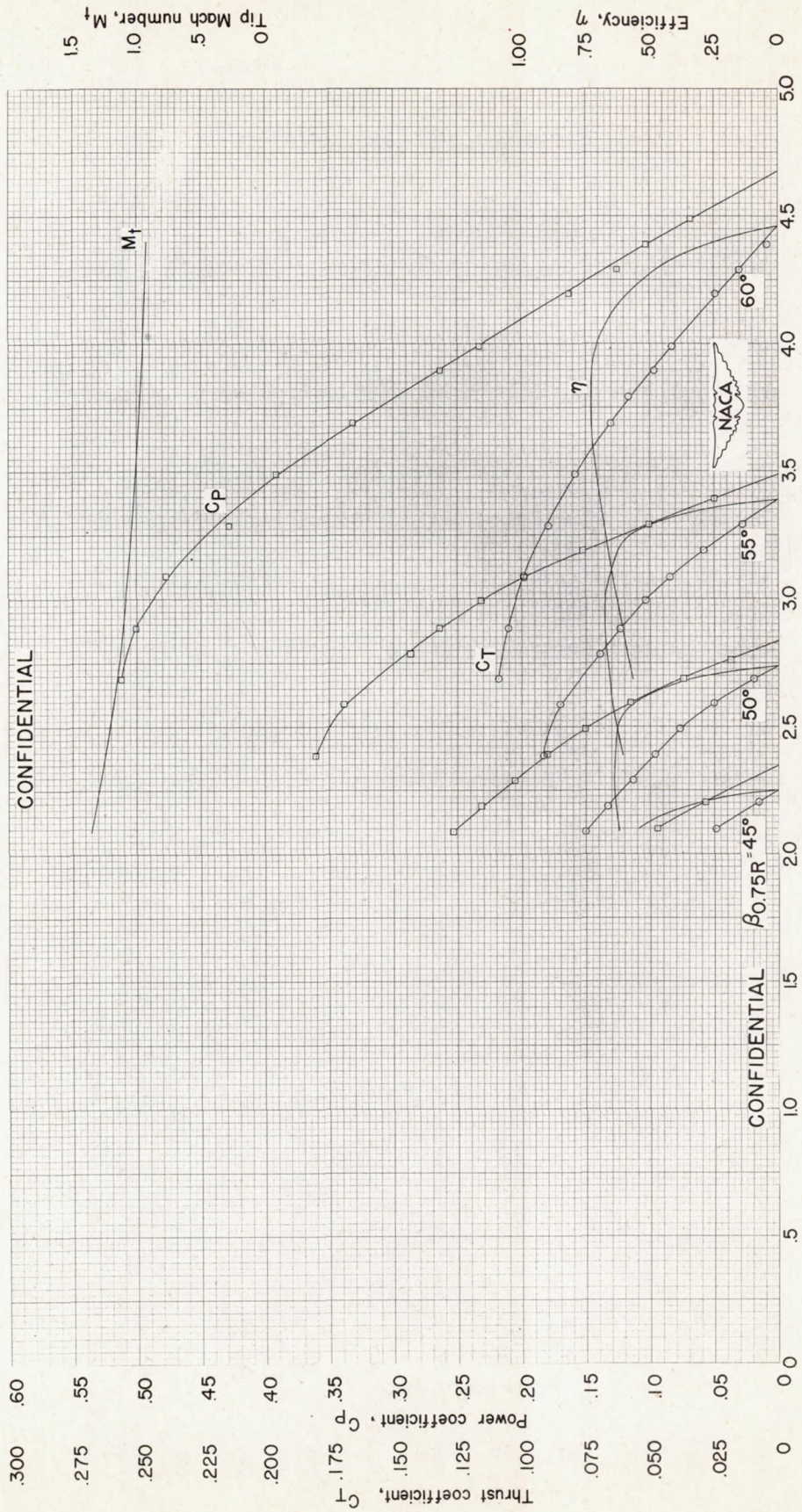

Figure 10 - Continued.

(i) M=0.75.

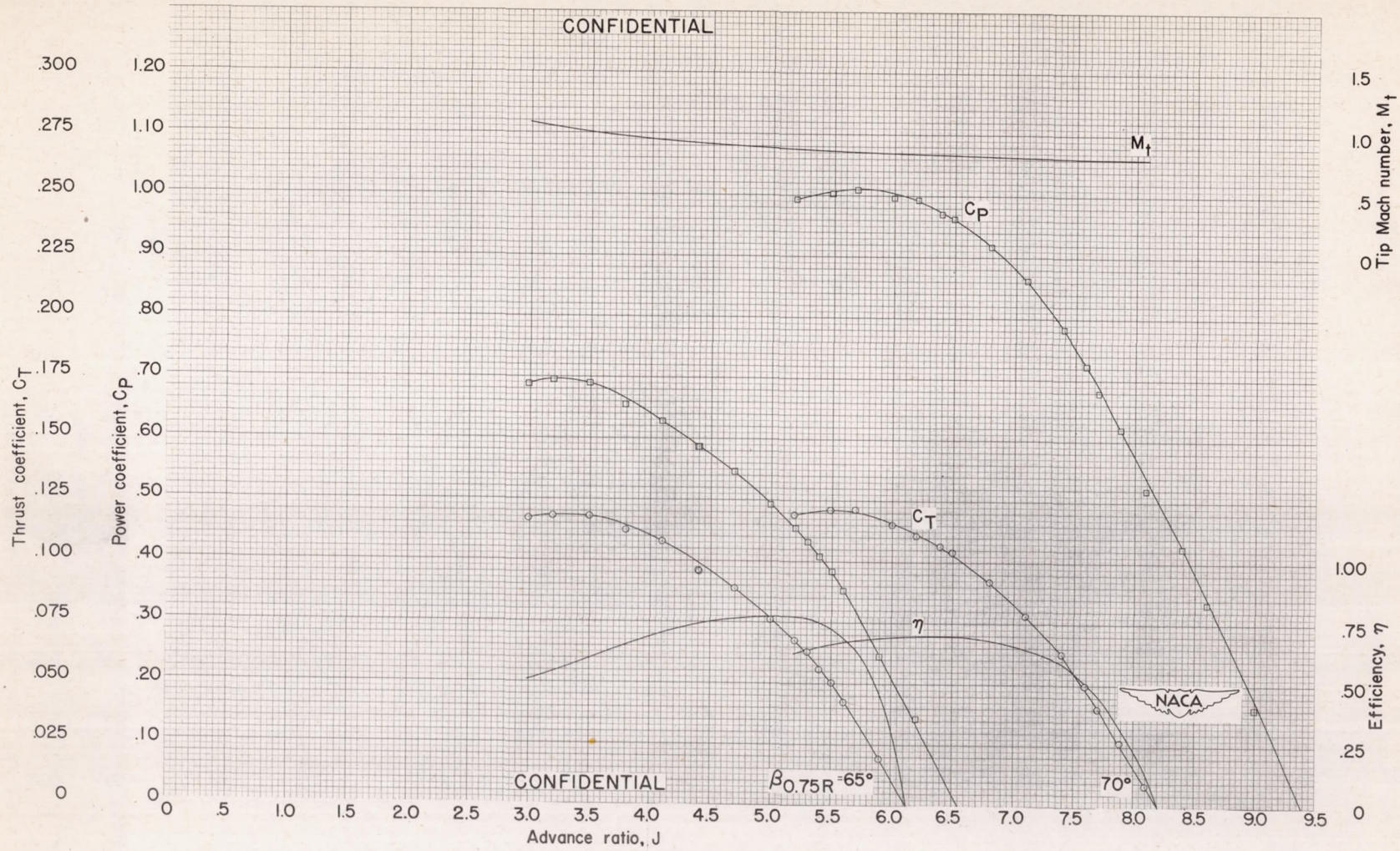

(i) M=0.75. Concluded.

Figure 10 - Continued.

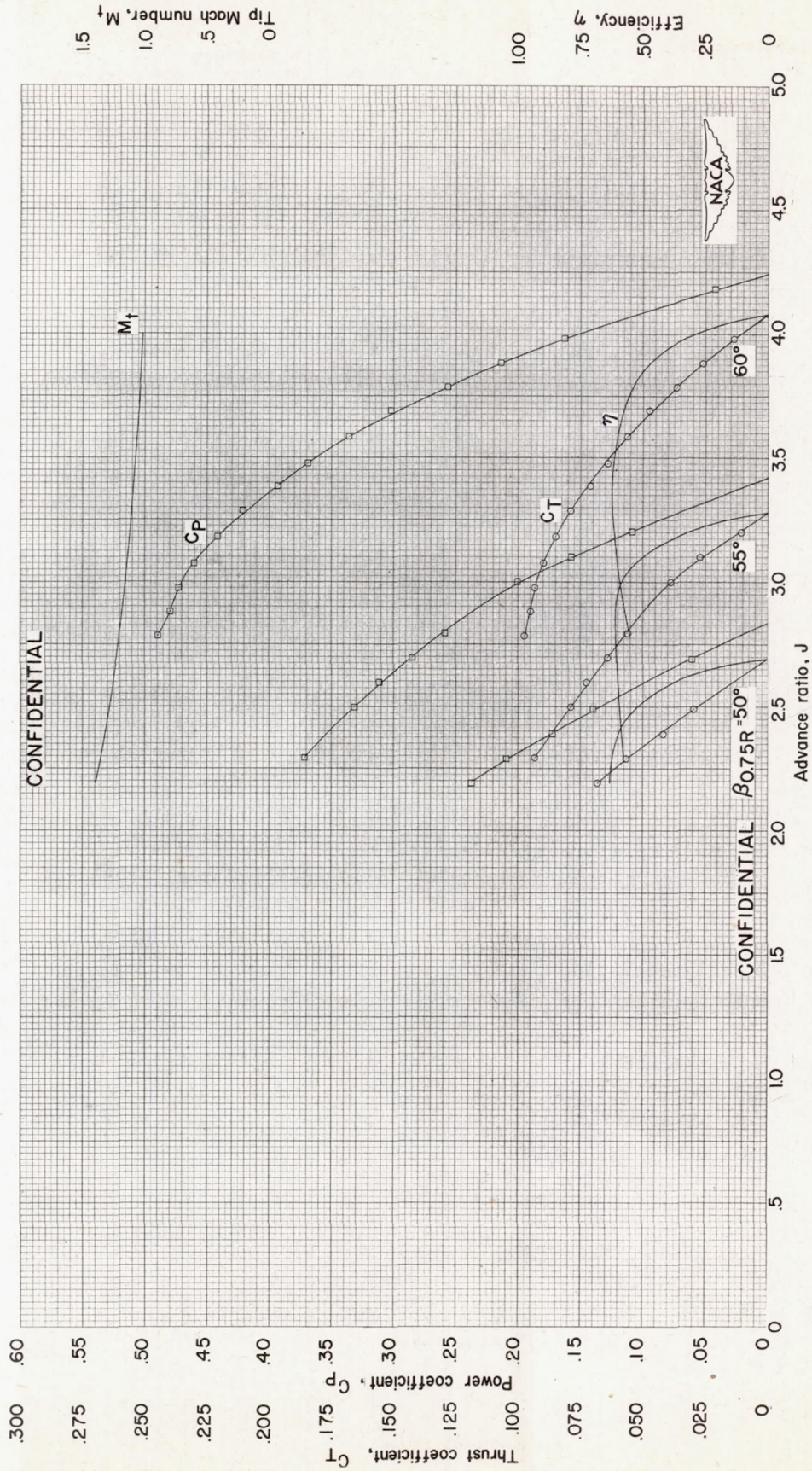

Figure 10 - Continued.

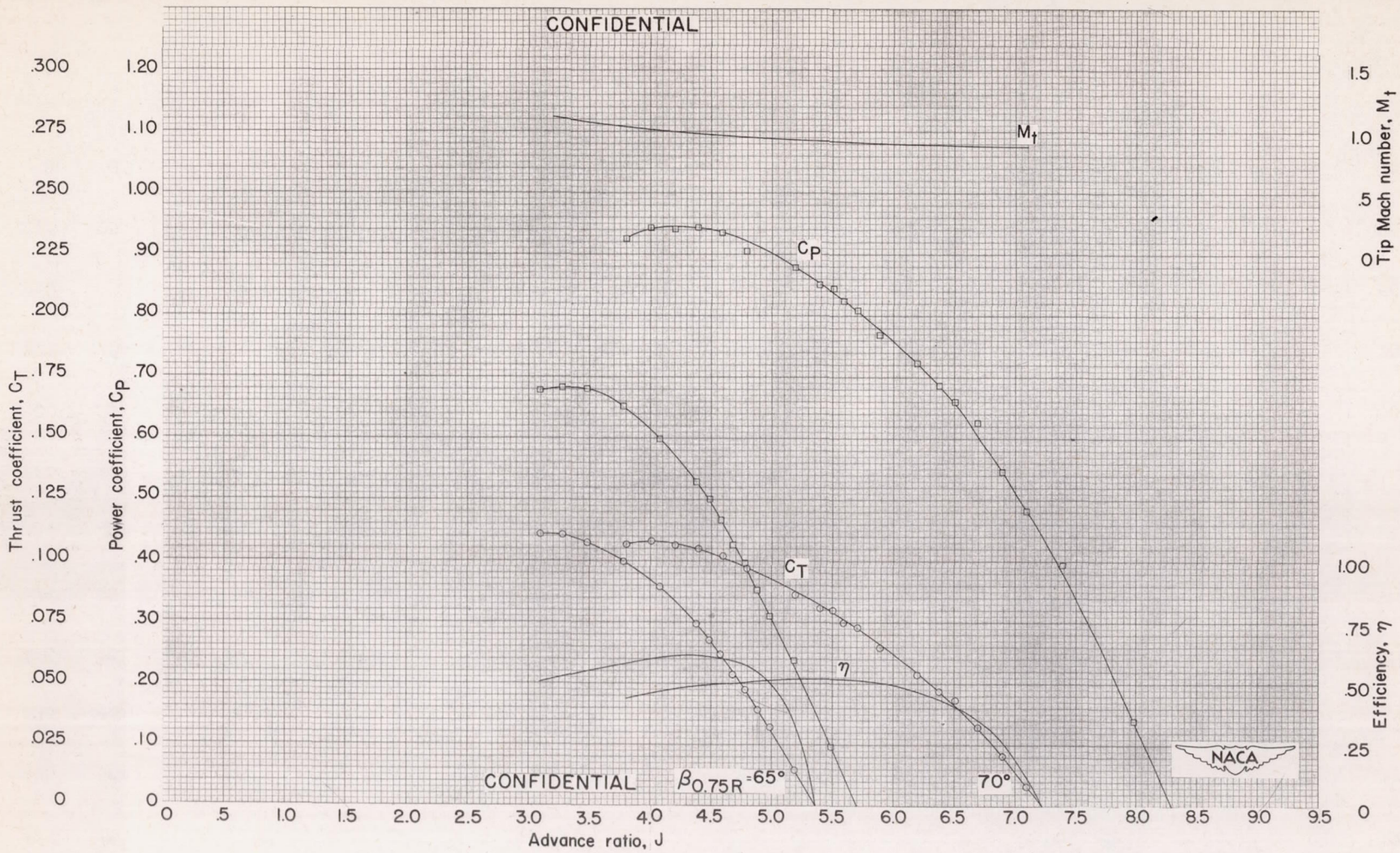

(j) M=0.80. Concluded.

Figure 10 - Continued.

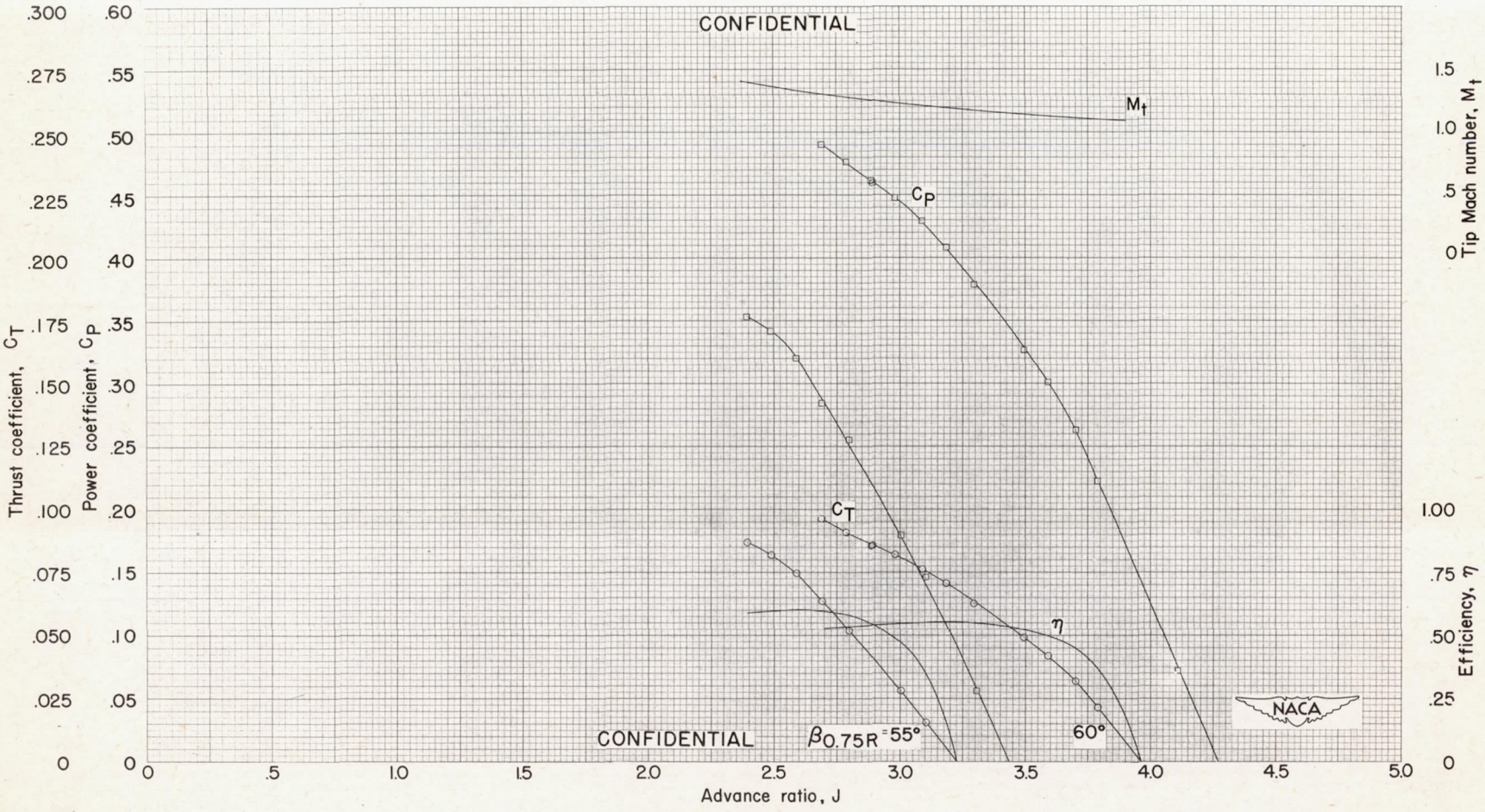

(k) M=0.85.

Figure 10 .- Continued.

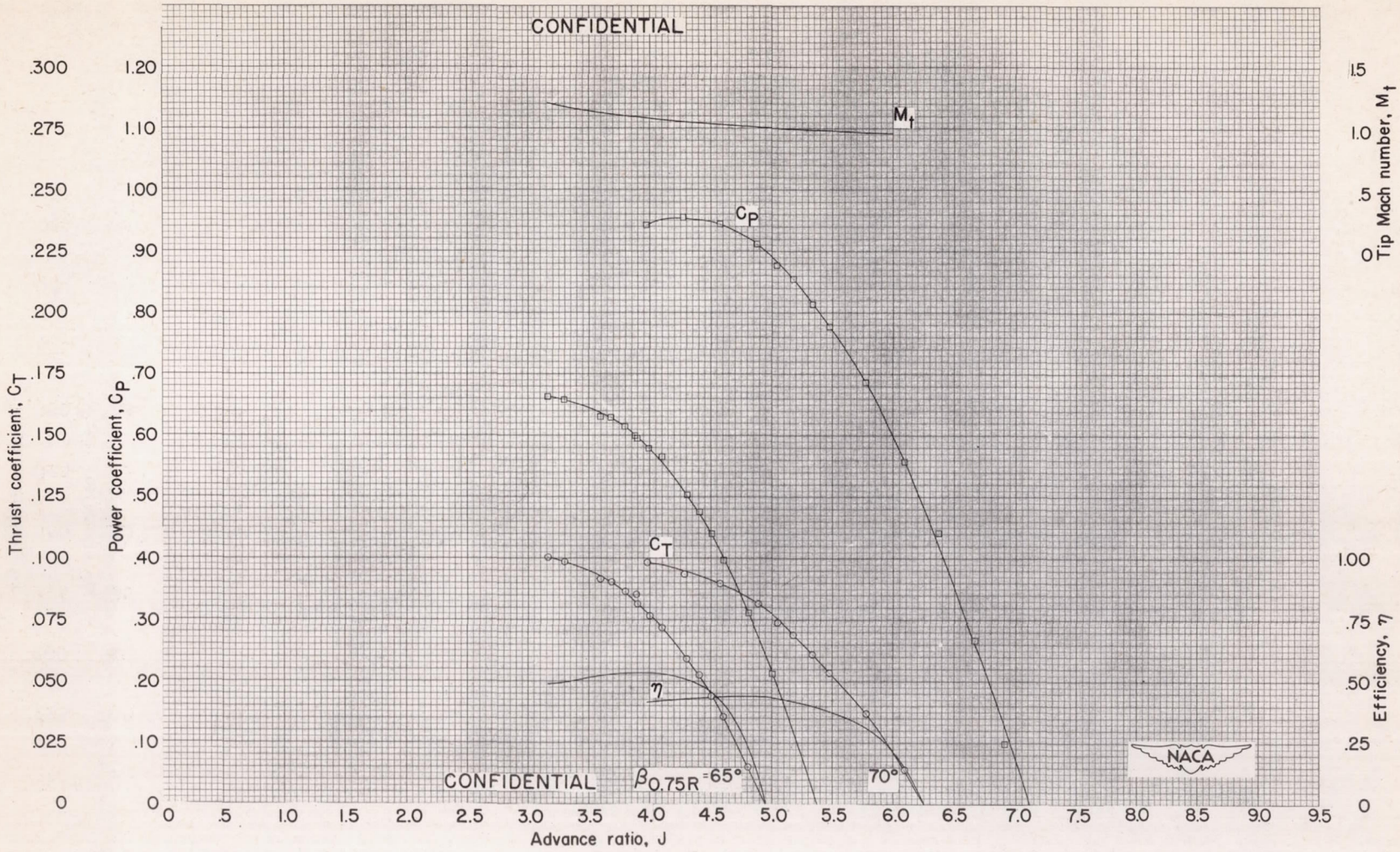

(k) M=0.85. Concluded.

Figure 10 .- Continued.

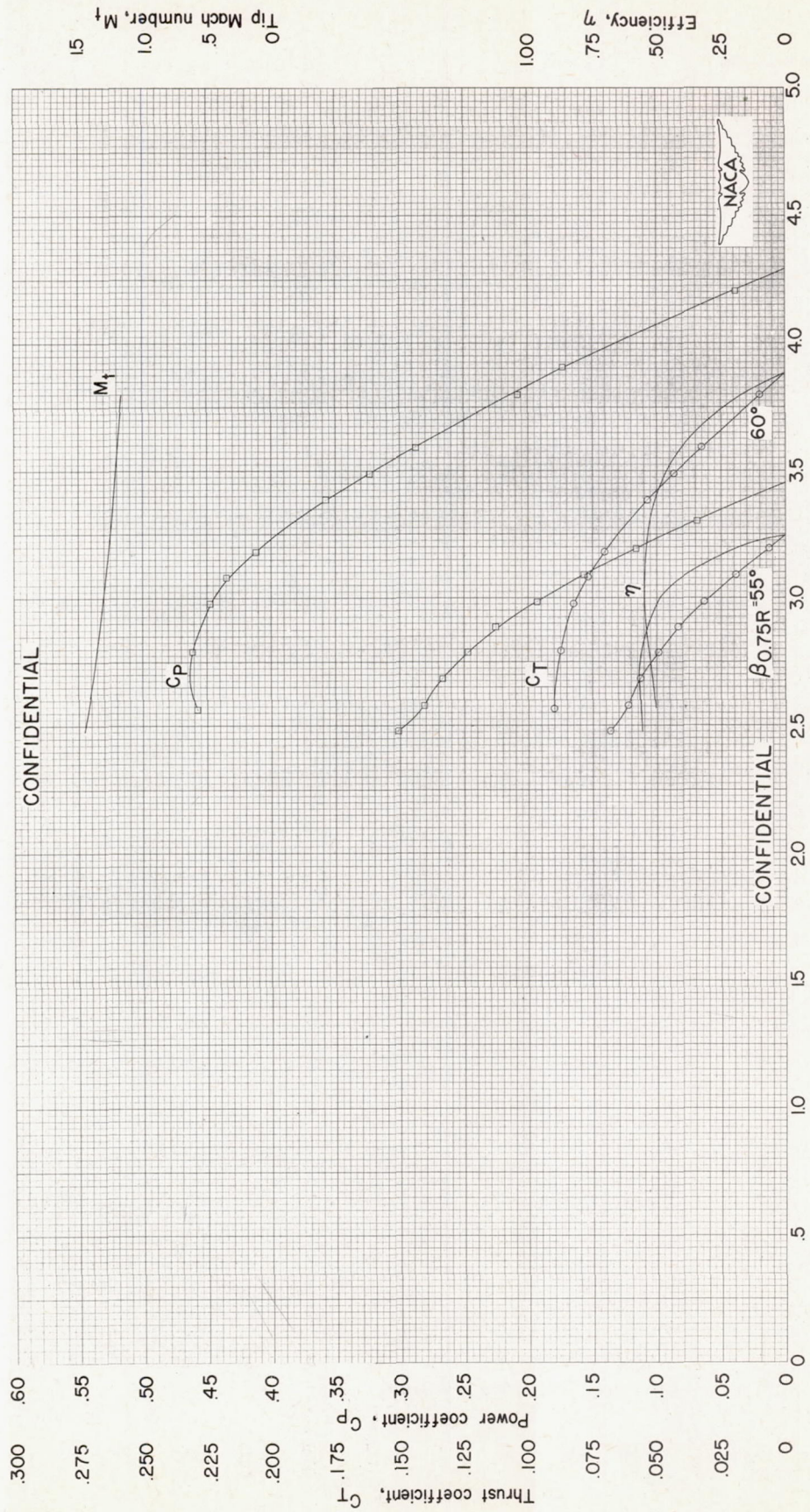

Figure 10 - Continued.

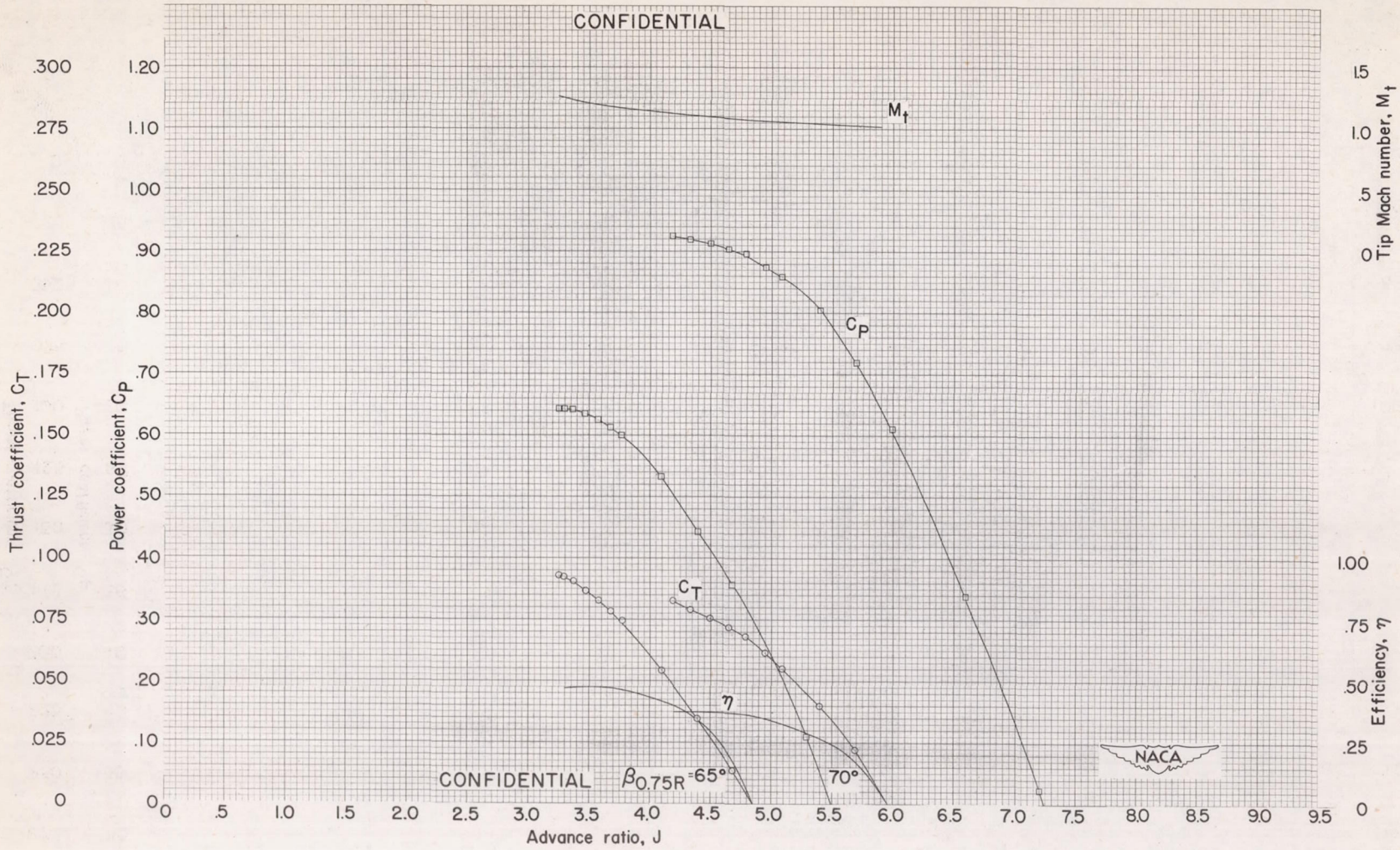

(1) M=0.90. Concluded.

Figure 10 - Continued.

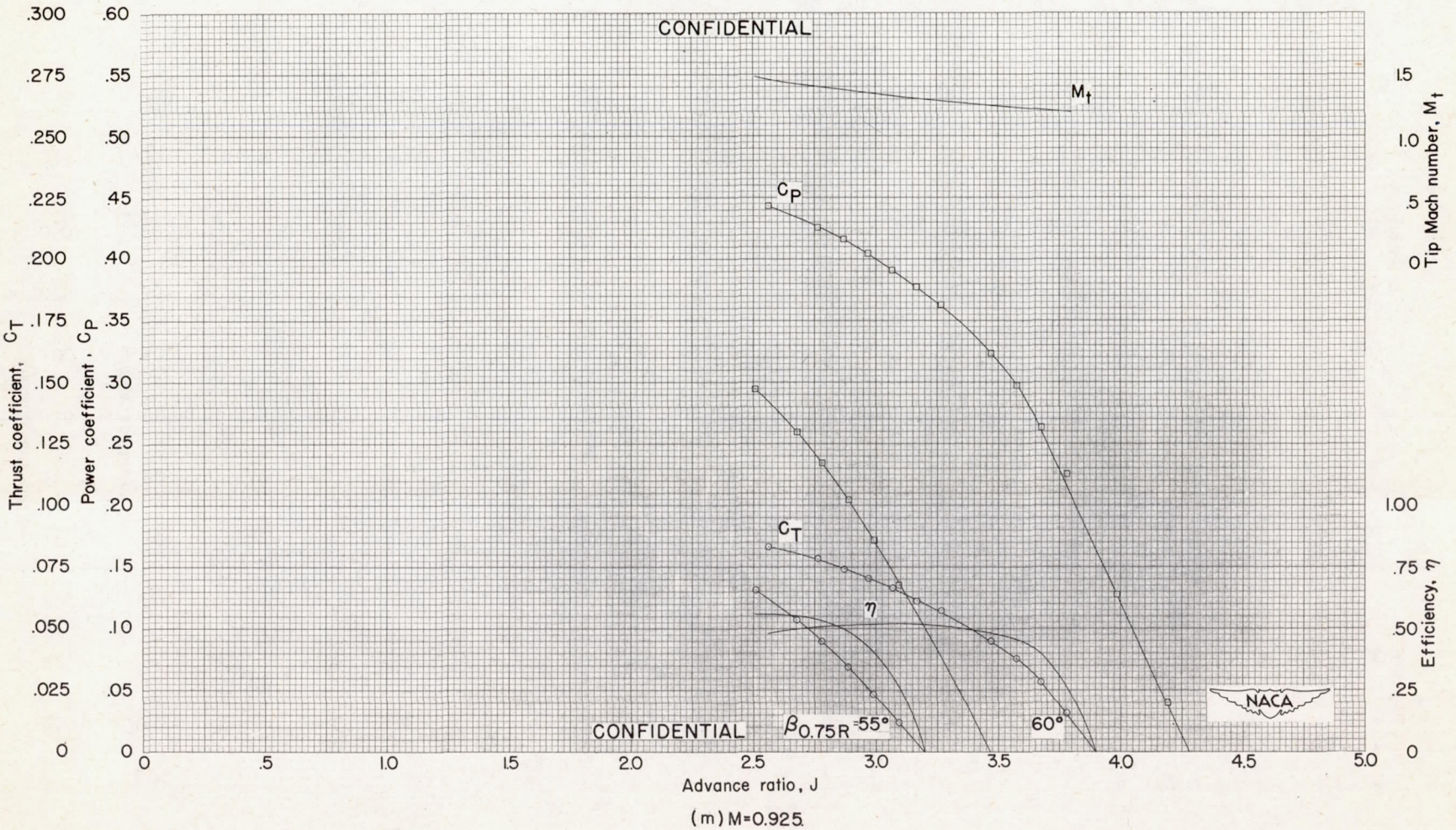

(m) M=0.925

Figure 10 - Continued.

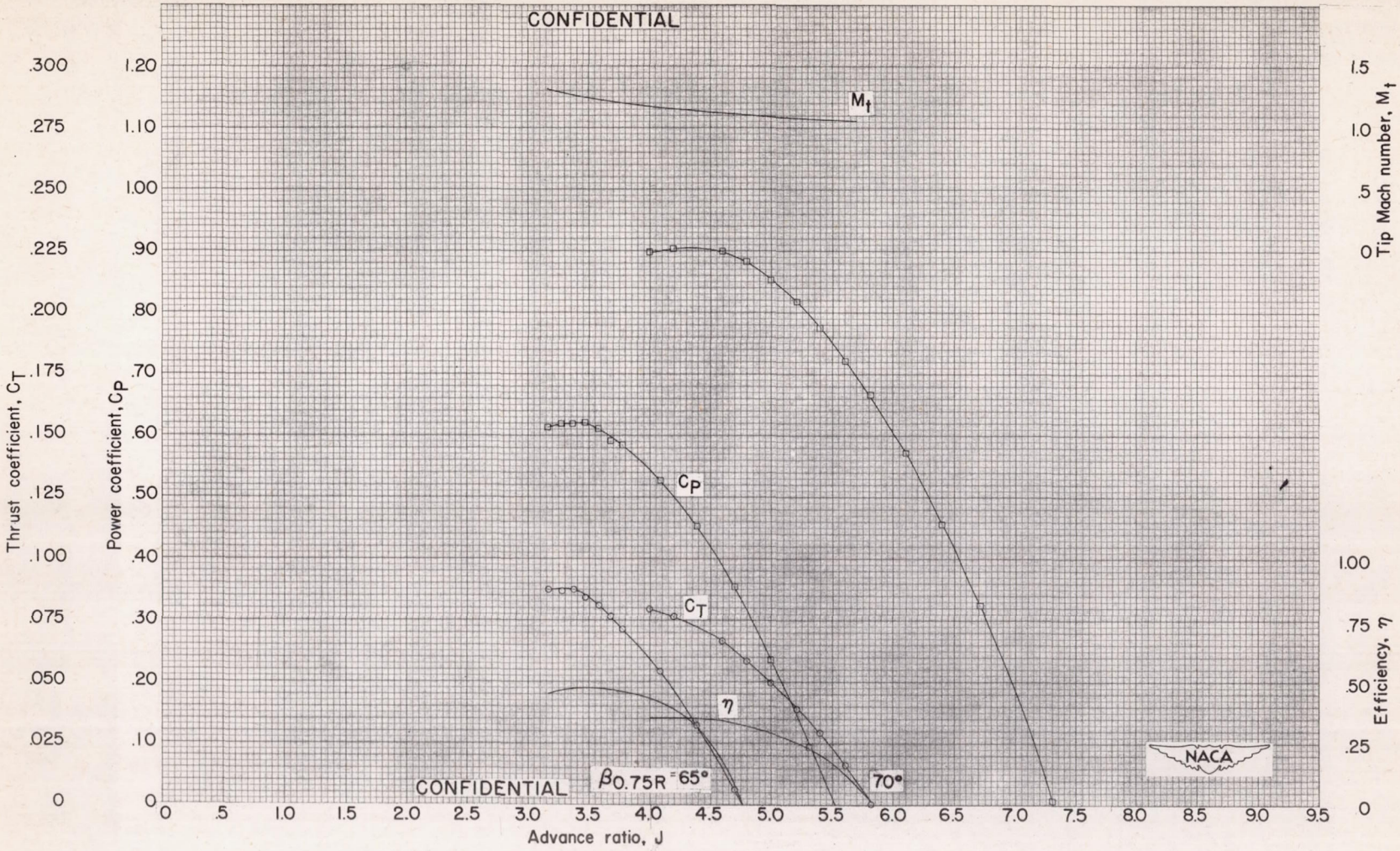

(m) M=0.925. Concluded.

Figure 10 - Concluded.

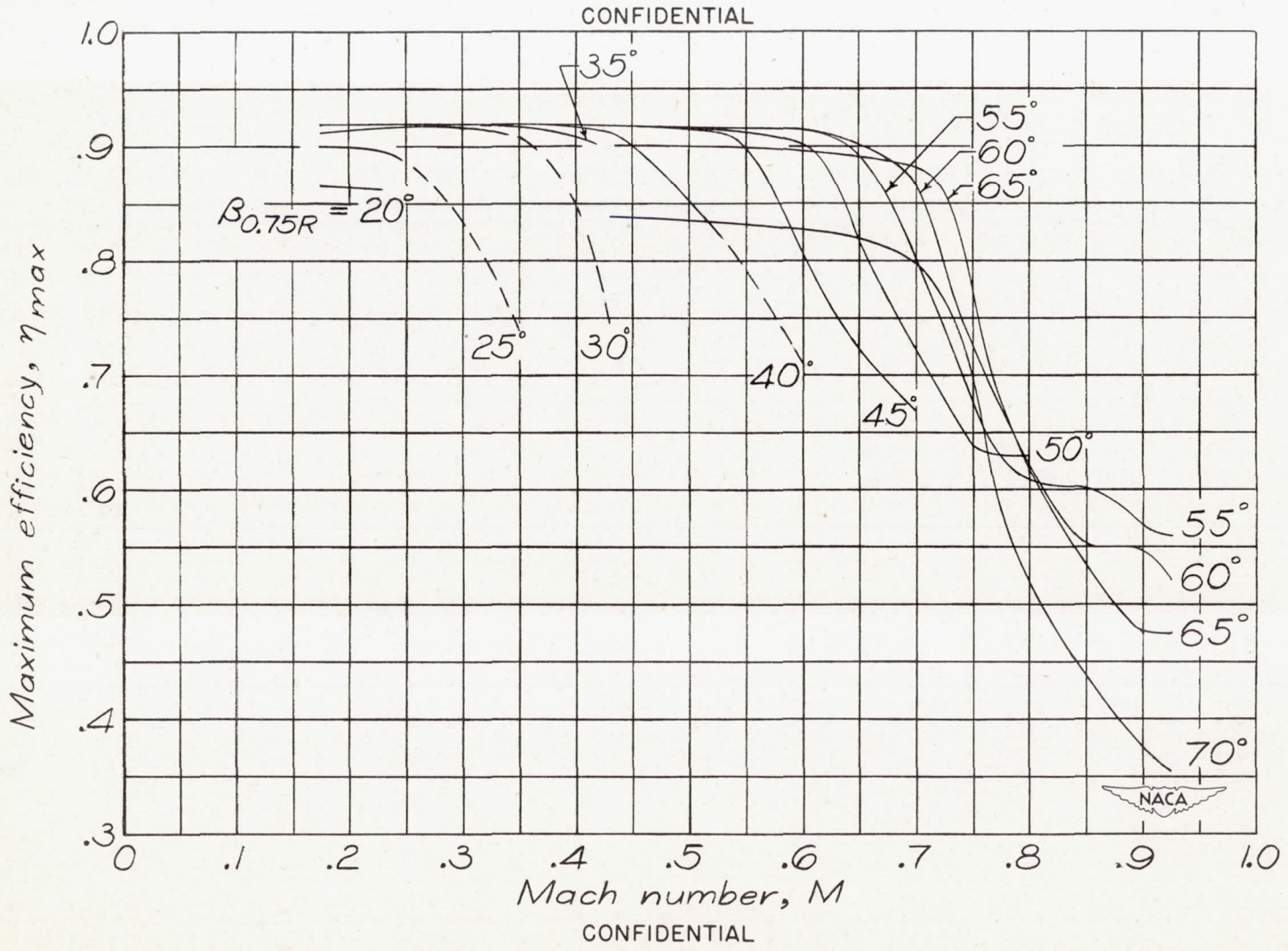

Figure 11.- Effect of forward Mach number on maximum efficiency. (Dashed lines indicate maximum efficiency was not attained.)

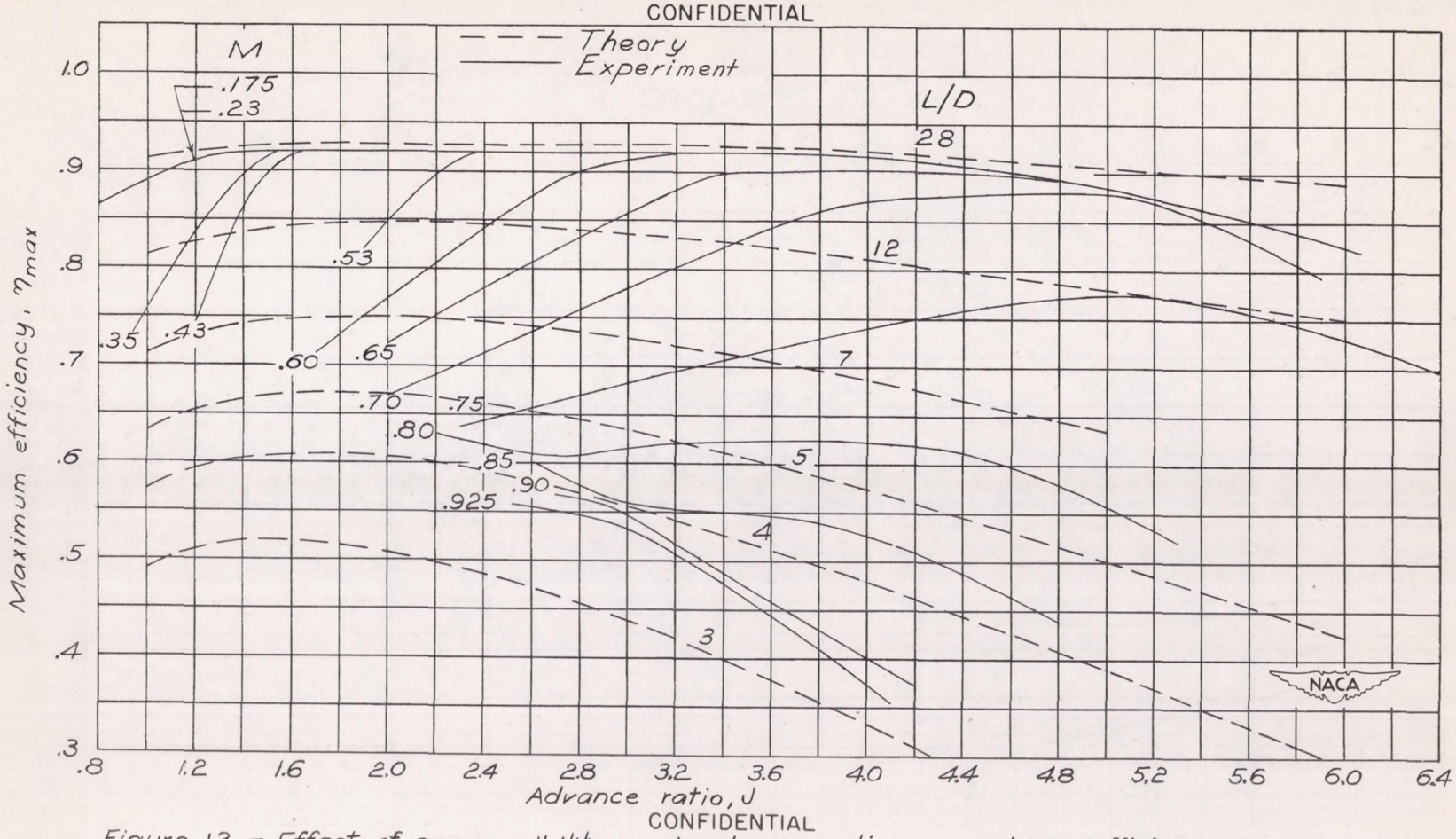

Figure 12.- Effect of compressibility and advance ratio on maximum efficiency.

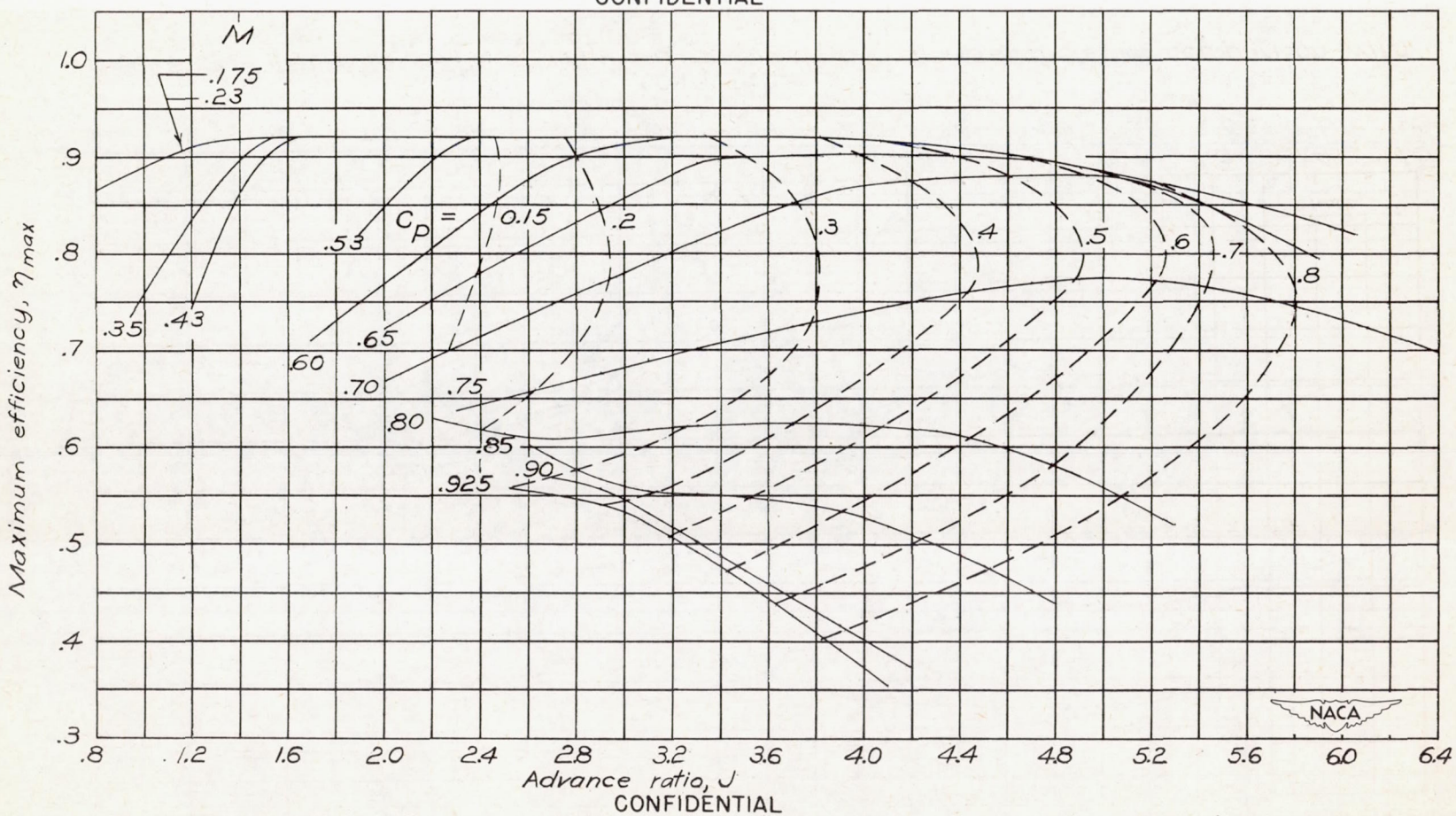

Figure 13.- Effect of compressibility and advance ratio on power coefficient for maximum efficiency

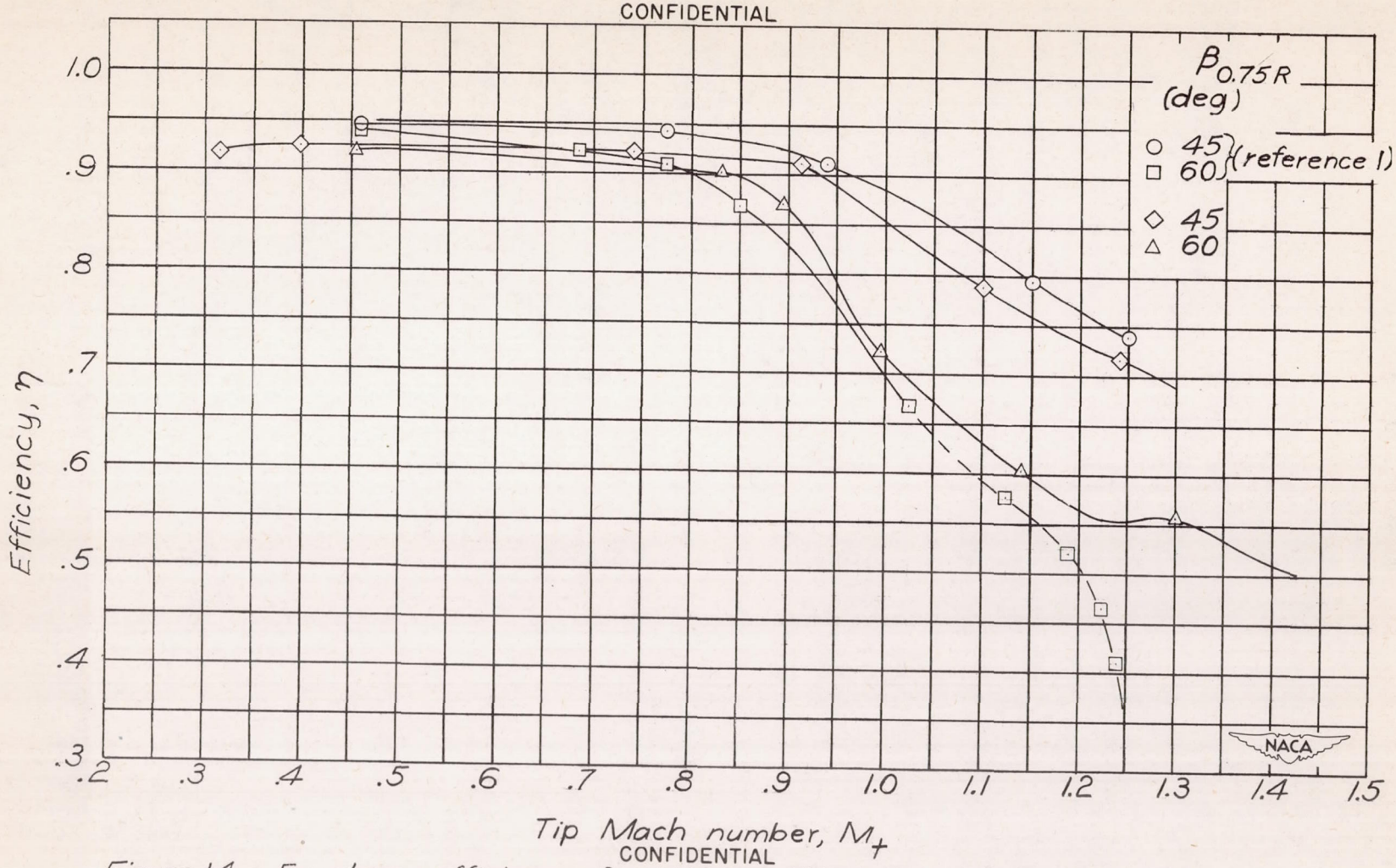

Figure 14. - Envelope efficiency for NACA 4-(5)(08)-03 propeller and comparison with results of previous investigation.